



Permafrost degradation and its consequences for carbon storage in soils of Interior Alaska

Patrick Liebmann · Jiří Bárta · Cordula Vogel · Tim Urich · Alexander Kholodov · Milan Varsadiya · Ole Mewes · Stefan Dultz · Muhammad Waqas · Haitao Wang · Olga Shibistova · Georg Guggenberger

Received: 21 July 2023 / Accepted: 13 February 2024 / Published online: 9 March 2024
© The Author(s) 2024

Abstract Permafrost soils in the northern hemisphere are known to harbor large amounts of soil organic matter (SOM). Global climate warming endangers this stable soil organic carbon (SOC) pool by triggering permafrost thaw and deepening the active layer, while at the same time progressing soil formation. But depending, e.g., on ice content or drainage, conditions in the degraded permafrost can range from water-saturated/anoxic to dry/oxic, with concomitant shifts in SOM stabilizing mechanisms.

Supplementary Information The online version contains supplementary material available at <https://doi.org/10.1007/s10533-024-01132-4>.

Responsible Editor: Brian Branfireun.

P. Liebmann (✉) · O. Mewes · S. Dultz · O. Shibistova · G. Guggenberger
Institute of Earth System Sciences, Section Soil Sciences, Leibniz University Hannover, Hannover, Germany
e-mail: liebmann@ifbk.uni-hannover.de

J. Bárta · M. Varsadiya · M. Waqas
Department of Ecosystem Biology, University of South Bohemia, České Budějovice, Czech Republic

J. Bárta
Faculty of Science, Centre for Polar Ecology, University of South Bohemia, České Budějovice, Czech Republic

C. Vogel
Institute of Soil Science and Site Ecology, Chair of Soil Resources and Land Use, Technical University Dresden, Tharandt, Germany

In this field study in Interior Alaska, we investigated two sites featuring degraded permafrost, one water-saturated and the other well-drained, alongside a third site with intact permafrost. Soil aggregate- and density fractions highlighted that permafrost thaw promoted macroaggregate formation, amplified by the incorporation of particulate organic matter, in topsoils of both degradation sites, thus potentially counteracting a decrease in topsoil SOC induced by the permafrost thawing. However, the subsoils were found to store notably less SOC than the intact permafrost in all fractions of both degradation sites. Our investigations revealed up to net 75% smaller SOC storage in the upper 100 cm of degraded permafrost soils as compared to the intact one, predominantly related to

T. Urich · H. Wang
Institute of Microbiology, University of Greifswald, Greifswald, Germany

A. Kholodov
Geophysical Institute, University of Alaska Fairbanks, Fairbanks, USA

M. Varsadiya
Ecological Microbiology, Bayreuth Center of Ecology and Environmental Research, University of Bayreuth, Bayreuth, Germany

the subsoils, while differences between soils of wet and dry degraded landscapes were minor. This study provides evidence that the consideration of different permafrost degradation landscapes and the employment of soil fractionation techniques is a useful combination to investigate soil development and SOM stabilization processes in this sensitive ecosystem.

Keywords Climate change · Permafrost thaw · Soil development · Soil organic matter · Soil fractions · Microbial decomposition

Introduction

Permafrost shapes large areas in polar regions of the northern and southern hemispheres and is characterized by consisting of permanently frozen soil ($<0\text{ }^{\circ}\text{C}$) for two or more consecutive years below a shallow seasonally thawed active layer (IUSS Working Group WRB 2022). Global warming disproportionately affects the sensitive arctic regions (Post et al. 2019), and undeniable landscape changes have been observed and reported in past decades (Jorgenson et al. 2006; Farquharson et al. 2019, 2022). Estimations demonstrate that a global temperature increase of $2\text{ }^{\circ}\text{C}$ could reduce the northern hemisphere permafrost areas by over 40% within the next century (Chadburn et al. 2017; Karjalainen et al. 2020). Currently, temperature development within the permafrost layer indicates a mean warming of $0.29 \pm 0.12\text{ }^{\circ}\text{C}$ across all permafrost regions, as observed for the period 2007–2016 (Biskaborn et al. 2019). This increase may seem relatively small, but, e.g., for the discontinuous permafrost areas of Interior Alaska, this corresponds to an active layer increase of $>3\text{ cm yr}^{-1}$ (Yi et al. 2018) and, in some areas, detachment of the active layer from permafrost table and formation of taliks, i.e., a perennially unfrozen layer of soil (Farquharson et al. 2022).

Deepening of the active layer has manifold consequences for soil and landscape development, for example, a change in aboveground vegetation and enhancement of plant rooting depth (i.e., Blume-Werry et al. 2019; Ogden et al. 2023). In turn, vegetation productivity can affect the temporal dynamic of permafrost thaw since a thicker vegetation cover can reduce thawing in the summer, whereas the warmer temperatures in winter caused by the increasing

thickness of the snow cover mitigate permafrost recovery due to isolation effects (e.g., Atchley et al. 2016; Heijmans et al. 2022). Deepening of the active layer increases the availability and mobilization of soil organic carbon (SOC), previously preserved in the frozen environment. Stabilization of vast amounts of SOC is maintained by an inhibited decomposition of organic matter (OM) in cold soils within the permafrost domain (Hobbie et al. 2000; Schuur et al. 2015). But ongoing ground warming reduces this natural protection, thus accelerating microbial OM decomposition and release of CO_2 and CH_4 to the atmosphere as well as mobilization and translocation of dissolved organic matter (DOM) and particulate organic matter (POM) to nearby surface waters (e.g., Estop-Aragonés et al. 2020; Gagné et al. 2020; Miner et al. 2022). Eventually, the large SOC storage in permafrost soils, with estimations ranging from 1000 to 1700 Gt (Zimov et al. 2006; Tarnocai et al. 2009; Hugelius et al. 2014; Friedlingstein et al. 2022), is at stake.

One well documented consequence of permafrost thaw is the collapse of the ground surface due to the melting of massive ground ice such as ice wedges or layers of ice-rich frozen deposits and the evolution of thermokarst lakes, which already cover large areas of northern polar regions (Jorgenson et al. 2006; Olefeldt et al. 2016; in't Zandt et al. 2020). In such landscapes, poorly drained soils, e.g., in proximity to thermokarst lakes, have a thicker active layer than intact permafrost soils, which could liberate parts of the thawed soil organic matter (SOM) (Textor et al. 2019). Accordingly, thawed mineral soil showed large SOC losses when soil water contents increased during tundra permafrost degradation (Hicks Pries et al. 2013). However, comparably cold and largely anoxic conditions in this wet landscape may hamper the effectivity of microbial decomposition (Bockheim and Hinkel 2007). Sometimes also both, as O'Donnell et al. (2012) showed that permafrost thaw in Alaskan peatland areas with limited drainage and accordingly large water contents resulted in accumulation of surface SOM, while thawed SOM in the subsoil was prone to microbial decomposition, thus resulting in a net loss of OC in the peat-rich active layer. Depending on ground ice content, texture, geomorphologic features, hydraulic connectivity, and vegetation cover (i.e., evapotranspiration), drainage

after permafrost thaw can also foster the development of dry landscapes with well-drained and oxic soils (Jorgenson and Osterkamp 2005; Ping et al. 2015; Estop-Aragonés et al. 2020; Jones et al. 2022; Jin et al. 2022). Under dry and warm conditions, microbial turnover of SOM is faster and more effective (Natali et al. 2015). But on the contrary, soil development, i.e., the formation of oxyhydroxides and soil aggregates, is likewise enhanced (Opfergelt 2020). Aggregate formation is facilitated by the interplay of mineral particles, OM, and microorganisms (Totsche et al. 2018) and can physically protect OM from decomposition by occlusion inside aggregates (Totsche et al. 2018; Opfergelt 2020). Iron-containing oxyhydroxide formation in aerobic parts of the soil (oxidation of reduced iron) can further provide physico-chemical protection of OM due to interactions of OM with the reactive mineral surfaces, thus forming mineral-organic associations (Kleber et al. 2007; Abramoff et al. 2021). This eventually can result in increased retention and stabilization of mobilizable SOM compounds as well as microbial metabolites (Wang et al. 2017), also in thawing permafrost soils (Gentsch et al. 2018; Liu et al. 2022). Previously, drying of degraded permafrost soils was found to intensify SOM turnover in the topsoil, while reducing decomposition rates of old SOM in the subsoil (Göckede et al. 2019; Kwon et al. 2019). Other studies suggest that the microbial community responds and adapts within years to permafrost thaw and that SOM decomposition can be increased under both aerobic and anaerobic conditions (Xue et al. 2016).

Even though it is certain that water-logged conditions in degraded permafrost soils, e.g., as a consequence of adjacent thermokarst development, significantly enhance the deepening of the active layer compared to well-drained permafrost-degraded soils (Nitzbon et al. 2020), the shift in SOM stabilization processes in degraded permafrost soils is often not considered in the current discussion. Furthermore, a potential long-term perspective with ongoing climate warming is not only considering permafrost degradation with more water-saturated soils, but also that more lakes and wetlands could disappear due to drainage (in't Zandt et al. 2020; Jones et al. 2022). An evaluation of contrasting permafrost degradation landscapes under dry and wet conditions is

still lacking more field evidence to resolve the fate of SOM during permafrost degradation.

In this study, the main objective was to evaluate SOM storage of soils in both a water-saturated (wet) and well-drained (dry) permafrost degradation landscape in comparison with an intact permafrost soil. We hypothesized that:

- (1) Differences in SOC between intact and degraded permafrost soils occur primarily in the subsoil, while in the topsoil stabilization processes associated with soil development mitigate the decline in SOC stocks.
- (2) Soil hydrological conditions determine whether inhibition of microbial decomposition (wet) or protection in aggregates and at mineral surfaces (dry) is maintaining SOM stabilization after permafrost degradation, but SOM preservation is not favored in soils from either degradation landscape.

For this, we selected three sites in a forested area underlain by discontinuous permafrost in the vicinity of Fairbanks, Alaska, where intact permafrost and degraded permafrost with wet and dry conditions is present within one kilometer distance and are not affected by different local climate conditions. Disentangling SOM stabilization mechanisms was done by sequential soil fractionation by aggregate size and particle density, followed by soil fraction-resolved quantification of C stocks and evaluation of the degradation stage of SOM.

Material and methods

Study sites

The study area is located in Interior Alaska, USA, at the city of Fairbanks. This research area belongs to the University of Alaska Fairbanks and provides different permafrost degradation landscapes within a few kilometers (Fig. 1a), thus ensuring comparable parent material and climatic conditions for soil development. The mean annual temperature in the research area is about -3 °C, and annual precipitation amounts to 500 mm (Rooney et al. 2023). The Fairbanks area is covered by Quaternary, Pleistocene and Tertiary glacial loess deposits (Fig. 1b; Rieger et al. 1963; Wilson

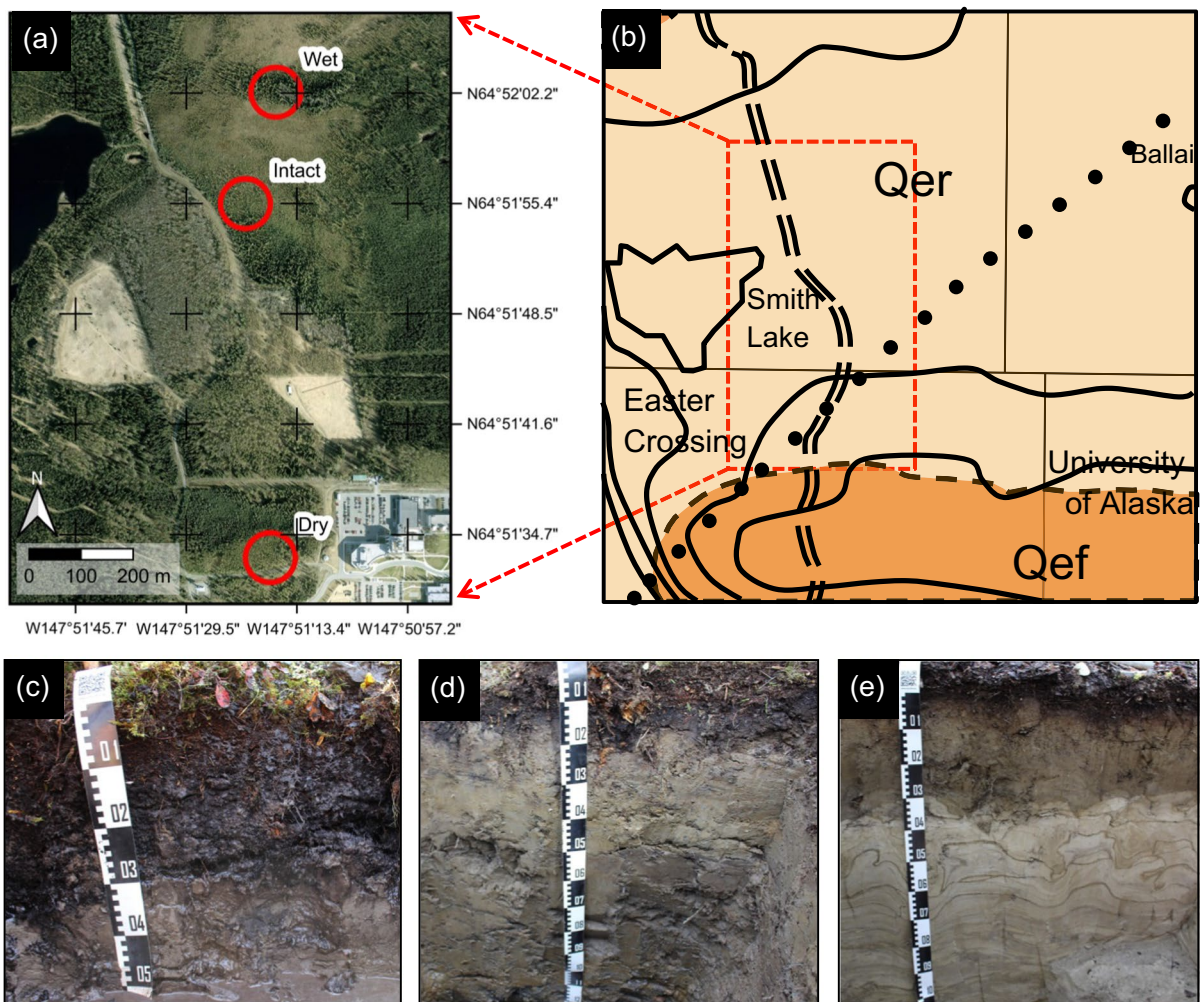


Fig. 1 Overview of the research area and the location of the three study sites intact permafrost (Intact), wet-degraded site (Wet), and dry-degraded site (Dry) is provided in (a) (Picture © 2023 Airbus, CNES/AirbusMaxar Technologies, Mapdata: Google© 2023). A geologic map section is provided in (b) [modified from Newberry et al. (1996)], with the contours of the Smith Lake on the left side and University Campus on the bottom. The area framed by the red-dashed line represents the dimensions of the research area shown in (a). The orange colored area at the bottom of the geologic map refers to the “Fairbanks Loess” deposits (abbreviation in map: Qef), whereas the bright orange colored area refers to re-transported

silt material originated from the same “Fairbanks loess” (abbreviation in map: Qer). Profile pictures of soils from the Intact permafrost (c) and both permafrost degradation landscapes (Wet (d), Dry (e)) in the Fairbanks research area are provided in the bottom part of the figure. The soil type at the Intact permafrost site was classified as Turbic Oxyaquic Histic Cryosol (Siltic, Eutric, Endic, Humic) (c). The Wet landscape was dominated by Turbic Reductaquic Cryosol (Eutric, Siltic) (d), and the Dry landscape was dominated by Dystric Regosol (Siltic, Nechic) (e). Note that the dark color of the Regosol topsoil (ca. 0–30 cm) is due to the infiltration of water from a precipitation event shortly before fieldwork started

et al. 2015). The loess deposits are underlain by schist and quartzite (Rieger et al. 1963).

Three landscape types with intact permafrost and two different permafrost degradation conditions were identified and selected for investigating the effects of permafrost thaw on soil development and

C retention and stabilization. The research area represents a north-facing gentle slope with the bottom being a depression between two lakes. The area is characterized by discontinuous permafrost distribution (Jorgenson et al. 2008). Permafrost temperatures vary from -2.5 to -0.5 °C. Within the degraded

permafrost areas, ground temperatures range from 1.9 °C (wet site) to 2.7 °C (dry site) (data not shown).

Intact permafrost landscape

A landscape consisting of intact permafrost soils with a shallow permafrost table and no major degradation features was selected as a reference (hereon, Intact permafrost). The plot is located at the toeslope with a north-facing aspect in close vicinity to Smith Lake (64° 51' 56.1" N 147° 51' 18.9" W). The tree vegetation is dominated by retarded growing conifers adapted to cold soils (primarily black spruce (*Picea mariana*) and tamarack (*Larix laricina*), and the forest floor vegetation is dominated by tussock wetland plants and includes ericoid shrubs, grasses, sedges, mosses, and lichens (Douglas et al. 2008). The soil was classified as a Turbic Oxyaquic Histic Cryosol (Siltic, Eutric, Endic, Humic) (Fig. 1c; IUSS Working Group WRB 2022). Specific features of this soil were different peat layers of 33 cm total thickness on top of the mineral horizons (Table 1), the presence of cryoturbated OM in various soil depths, and predominantly oxic pore water in the thawed mineral soil (redox potential > 500 mV) determined by stationary redox potential measurements (data not shown). The thaw depth at the moment of sampling varied between 45 and 55 cm.

Wet landscape

A landscape consisting of degraded permafrost soils with large water contents (hereon, Wet site) was selected within 200 m distance north of the Intact permafrost (64° 52' 02.4" N 147° 51' 17.3" W). It is located on a low hill (difference in elevation between Wet site and the Intact permafrost is about 1–2 m) at the bottom of the depression between Smith and Balaine lakes. Thawing is accelerated due to higher impact of snowpack insulation during winter seasons because of more open conditions compared to the intact permafrost which results in less snow trapped on the tree canopies and thus higher snow accumulation at the ground. In addition, poor drainage leads to higher latent heat release during soil water freezing. The Wet site features characteristics of the “Irregular Thermokarst Mounds” permafrost mode, one of 14 primary permafrost modes of boreal Alaska described by Jorgenson and Osterkamp (2005). Even though

there is no lake development due to thermokarst at the research sites, the Wet site can be considered as a model of permafrost degradation due to the process of thermokarst. The forest at the site is also dominated by conifers [primarily black spruce (*Picea mariana*) and white spruce (*Picea glauca*)], but characterized by less stunted growth compared to the Intact permafrost. Within the plot, an intermittent of suppressed birch trees occurs. The forest floor vegetation is represented by ericoid shrubs, grasses, sedges, mosses, and lichens (Douglas et al. 2008). The soil was classified as a Turbic Reductaquic Cryosol (Eutric, Siltic) (Fig. 1d; IUSS Working Group WRB 2022) covered with an 11 cm thick organic layer (Table 1). The permafrost table varied between 100 and 200 cm soil depth, accompanied by cryoturbations in various depths within the upper 100 cm. The mottled upper mineral horizons display dynamic redox conditions in the topsoil, whereas in the subsoil, immediate ferrihydrite formation on the profile wall after soil profile excavation illustrates the reducing conditions (Fig. 1d).

Dry landscape

A landscape consisting of degraded permafrost soils, which are well aerated and have small water contents (Table 1), was selected about 700 m south of the Intact permafrost at the shoulder of a north-facing slope (64° 51' 33.5" N 147° 51' 18.0" W) (hereon, Dry site). The difference in elevation between the Dry site and the intact permafrost is about 35 m. The vegetation is dominated by deciduous trees (primarily birch (*Betula papyrifera*) and aspen (*Populus tremuloides*)). Shrubs, mosses, and lichens represent the forest floor vegetation. The soil was classified as a Dystric Regosol (Siltic, Nechic) (Fig. 1e; IUSS Working Group WRB 2022), covered with an 8 cm thick organic layer. The hilltop area experienced a disturbance in the first half of the twentieth century, but did not show permafrost degradation features observed at an agricultural test field (deforestation in 1908 and plowing in the 1940s years; Péwé 1954) in the same area such as 100–200 cm deep trenches separating mounds of 200–300 cm in diameter [personal observation; Polygonal Thermokarst Mounds (Jorgenson and Osterkamp 2005)]. We thus infer that disturbance in the Dry site area was limited to the removal of the

Table 1 Selected physico-chemical parameters of the different soil types at the Intact permafrost site (Turbic Oxyaquic Histic Cryosol (Siltic, Eutric, Endic, Humic); permafrost not degraded), and the two degradation landscapes Wet (Turbic Reductaquic Cryosol (Eutric, Siltic); permafrost degraded and water-saturated), and Dry (Dystric Regosol (Siltic, Nechic); permafrost degraded and drained)

Landscape	Horizon nomenclature*	Depth [cm]	BD [g cm ⁻³]	Water content [vol. %]	Soil temperature (°C)	pH [H ₂ O]	Clay [mg g ⁻¹]	Silt [mg g ⁻¹]	Sand [mg g ⁻¹]	OC [mg g ⁻¹]	TN [mg g ⁻¹]	Cations [cmol _c kg ⁻¹]	BS [%]
Intact	Hi	0–5	n.d.	n.d.	4.8	4.52	n.d.	n.d.	n.d.	401.78	9.34	25.14	85.42
	He	5–15	0.13	70.90	2.4	6.09	n.d.	n.d.	n.d.	376.27	11.20	51.18	91.93
	Ha	15–33	0.20	75.16	1.9	5.91	n.d.	n.d.	n.d.	345.71	14.48	72.74	89.67
	Cg@	33–45	1.26	57.01	0.6	6.05	131	776	93	22.74	1.52	23.80	47.86
	Cf@	45+	1.51	43.65	–0.3	6.13	150	769	81	27.47	1.88	25.65	49.39
	Oi	0–1	n.d.	n.d.	14.5	n.d.	n.d.	n.d.	n.d.	414.60	9.87	n.d.	n.d.
Wet	Oe	1–7	0.06 ^a	18.45 ^a	10.5	3.77	n.d.	n.d.	n.d.	413.31	10.79	22.93	68.77
	Oa	7–11	0.06 ^a	18.45 ^a	7.2	5.01	n.d.	n.d.	n.d.	281.02	12.08	43.89	75.25
	Ah	11–14	1.38	43.73	4.2	5.87	132	752	116	49.25	2.57	31.09	64.68
	Bw@	14–44	1.52	38.80	4.0	5.97	102	705	193	5.50	0.46	17.18	53.39
	Br@	44–73	1.42	44.58	3.4	5.99	92	750	158	4.98	0.50	15.25	54.08
	Cr@	73–100+	1.35	46.54	2.7	6.10	82	726	192	3.83	0.45	13.68	53.98
Dry	Oi	0–1	n.d.	n.d.	14.0	n.d.	n.d.	n.d.	n.d.	464.45	12.63	n.d.	n.d.
	Oe	1–3	0.14 ^a	24.18 ^a	13.0	4.57	n.d.	n.d.	n.d.	413.32	18.74	37.20	80.85
	Oa	3–8	0.14 ^a	24.18 ^a	11.5	4.17	n.d.	n.d.	n.d.	400.66	15.83	37.11	61.19
	AhE	8–8.5	1.09 ^b	35.82 ^b	10.5	4.34	n.d.	n.d.	n.d.	119.77	4.94	24.49	42.99
	AhBs	8.5–11	1.09 ^b	35.82 ^b	10.5	4.62	159	797	44	37.58	2.12	22.35	35.38
	Bw	11–13	1.09 ^b	35.82 ^b	9.8	4.86	145	789	66	18.24	1.20	21.78	31.57
BwC	BwC	13–21	1.42	33.49	9.6	5.40	119	812	69	5.70	0.50	19.84	39.42
	C1	21–35	1.45	33.94	8.6	5.81	142	799	59	3.88	0.46	20.99	52.46
	C2	35–100+	1.30	12.17	7.5	6.60	122	835	43	3.84	0.44	19.52	66.48

Horizon-specific features are stated within the horizon nomenclature, e.g. with the suffixes g (loss of Fe and Mn oxides on aggregate surfaces), f (frozen, permafrost), r (strong reduction), or @ (cryogenic alteration) (IUSS Working Group WRB 2022). Data include the bulk density (BD), organic carbon contents (OC), total nitrogen contents (TN), plant-available cations (Cations) and base saturation (BS) derived from Mehlich 3 extraction

n.d. not determined

* According to IUSS Working Group WRB (2022)

^a composite sample of Oe and Oa material

^b composite sample of AhE, AhBs, and Bw material

vegetation cover, either by human activities or by natural events like a wildfire, with no direct human intervention in the soil. No permafrost was recorded in the upper 200 cm of soil for at least the last 70 years (Péwé 1954). With this, the Dry site can be considered as a representative of boreal silty upland landscapes in Alaska (Jorgenson et al. 2013). The soil profile showed no signs of former cryoturbations, but contained lamellic illuvial clay (Fig. 1e), which illustrates the former illuviation of clay by infiltrating snowmelt and rainwater (about twice the clay content compared to the surrounding soil).

Study site comparability

The approach taken here makes use of comparable situations of the three study sites and a similar composition of the soils prior to the initiation of permafrost thaw. First of all, permafrost must have been present up to the backslope of the hill within the study area in the past. Rooney et al. (2023) reported on permafrost depths between 60 and 90 cm (from the soil surface) at all positions along a similar slope gradient in the Fairbanks area and together with our own observations of isolated permafrost spots within 100 m distance to the Dry site, we infer that permafrost was present prior to degradation. Second, the natural forest succession from spruce to birch/aspens mix deciduous forest was described for well-drained permafrost-free soils of Interior Alaska, whereas poorly drained sites are typically dominated by black spruce stands (Péwé 1954; Van Cleve and Viereck 1981; Jorgenson et al. 2010). Even though there is evidence of disturbance at the Dry site, forest succession apparently happened in a comparable way to the natural one, as this succession is largely based on deciduous trees growing faster than conifers (Mack et al. 2021). We thus can infer that the Dry site was likewise dominated by black spruce prior to permafrost thawing as well as the Wet site. Albeit we do not have ^{14}C ages of SOM from the Wet and Dry site, Waldrop et al. (2010) and Wickland et al. (2018) reported ^{14}C ages of SOM from the Smith Lake area (Intact permafrost) of 2000–3000 years (active layer) to 5000–6000 years (permafrost), thus suggesting that large parts of the accumulated OM in this area is older than the recent thawing event.

Sampling

The sampling campaign in Fairbanks was conducted at the maximum permafrost thaw depth in late August–early September 2021. At each site, one 150×100 cm profile was prepared with a depth of either 100 cm (Wet and Dry) or until reaching the permafrost table (Intact). Soil sampling was done per horizon by taking the material from three profile walls. This sampling scheme was chosen to evaluate changes within each horizon of the soil profiles as a consequence of permafrost thaw. For determining the bulk density and water content, the soil was additionally sampled in 100 cm⁻³ cylinders, weighted field fresh, and a 2nd time after 3 days of oven-drying at 65 °C. In order to assess soil processes behind SOC stock changes, evaluation of soil horizons alone was not suitable, as horizon development (e.g., change in thickness, bulk density, illuvial or eluvial processes) proceeds. Hence, in a second sampling, another three satellite soil pits were excavated within 10 m distance to the soil profile. Together with the soil profile pit, a total of four replicates of mineral topsoil (Topsoil) and mineral subsoil (Subsoil) material in defined soil depths within the active layer were sampled. With this, SOC stock changes were evaluated on the basis of the same mineral soil depth and especially within a uniform 5 cm thick depth increment. Mineral soil depths within the active layer were chosen since our approach was focused on aggregate- and oxyhydroxide formation linked to the overall decomposition of SOM, processes that take place in unfrozen soil. Thus, the Topsoil depth increment was defined from 2 to 7 cm below the organic layer to assure comparability between the three sites in terms of connectivity to the organic layer, since topsoils are typically classified according to the accumulation of OM. The Subsoil increment was defined from 45 to 50 cm below the organic layer, as degraded sites showed B- and C-horizons in this depth. For the shallow active layer of the intact permafrost, the Subsoil depth would have been within the frozen ground. But due to the restriction to the active layer, the maximum distance to the Topsoil depth was chosen, i.e., a 5 cm increment above the permafrost table, on average 10 cm below the Topsoil depth. A previous study reported that less degraded permafrost soils of a similar slope gradient in this area had about 40 cm of thawed mineral soil (Rooney et al. 2023). Hence, it can be expected that

the Subsoil depths of the degraded sites were located in the upper part of the permafrost table or within the transition zone between permafrost table and active layer prior to permafrost degradation, the latter would thus resemble the current situation in the Subsoil depth of the intact permafrost. An extension to Table 1, covering basic soil parameters of the Top- and Subsoil increments, is given in the supplementary information (Supplementary Table S1).

Physico-chemical analyses

After sampling, soil material for physico-chemical analyses was air-dried and sieved <2 mm. Soil pH was determined in suspension in ultra-pure H₂O (18.2 MΩ) with a soil-to-solution ratio of 1 to 2.5. Soil texture was analyzed according to DIN ISO 11277 (2002) after OM oxidation with 35% H₂O₂ and dispersion of soil aggregates with sodium metaphosphate. Analysis of the mineralogical composition of the clay fraction was performed according to Moore and Reynolds (1997). The clay fraction (<2 μm) was separated by sedimentation and decantation after the removal of OM with H₂O₂ (35%) and Fe oxides using dithionite-citrate-bicarbonate extraction. For X-ray diffractometry (XRD; D 500, Siemens, Munich, Germany; Cu Kα radiation, range of 1 to 30° 2θ), the clay samples were saturated with K⁺ and Mg²⁺, respectively. After removing free salts, the suspensions were transferred to glass slides and allowed to dry at room temperature. In addition, the K⁺-saturated sample was heated to 550 °C, and the Mg-treated sample was exposed to ethylene glycol vapor. Moreover, Fourier transform infrared (FTIR) spectroscopy in the range of 4000–400 cm⁻¹ was performed with the clay fraction in transmission mode using KBr pellets (Tensor 27, Bruker, Karlsruhe, Germany) (Lessovaia et al. 2014).

Aliquots were ground in a ball mill and weighted into tin capsules for SOC, total nitrogen (TN), and the bulk soil's ¹³C/¹²C ratio determination. Samples were measured by a vario ISOPRIME cube (Elementar Analysensysteme GmbH, Hanau, Germany) elemental analyzer coupled to an IsoPrime100 (IsoPrime Ltd, Cheadle Hulme, UK) stable isotope ratio mass spectrometer (EA-IRMS). Soil OC to TN ratios were calculated based on the measured C and N contents in mg g⁻¹. Carbon isotope values are given in the delta

notation relative to the Vienna Pee Dee Belemnite (VPDB; Hut (1987)).

Selective extractions were conducted to determine the content and specification of soil-borne iron (Fe) and aluminum (Al). Poorly crystalline aluminosilicates and Fe hydroxides (i.e. ferrihydrite), in addition to organically complexed Al (Al_o) and Fe (Fe_o) were dissolved by 0.2 M ammonium oxalate solution at pH 3, according to McKeague and Day (1966). Iron bound in organic complexes, poorly crystalline hydroxides and crystalline oxides (Fe_d) was dissolved by dithionite-citrate-bicarbonate solution following the method created by Mehra and Jackson (1960) and modified by Sheldrick and McKeague (1975). By subtracting the oxalate-extractable Fe from the dithionite-extractable Fe, an estimate of the more crystalline Fe phases (Fe_c) was done. Exchangeable cations were extracted by Mehlich 3 solution (Mehlich (1984); detailed method description in Carter and Gregorich (2008)), and comprised Na, K, Mg, Ca, Al, Fe, and Mn.

All extracts were measured by inductively coupled plasma optical emission spectroscopy (ICP-OES; Varian 725-ES, Palo Alto, CA, USA).

Total DNA and RNA extraction

Soil samples (appx. 3 g) were immersed with 2 volumes of LifeGuard Soil Preservation Solution (Qiagen, Hilden, Germany) directly in the field immediately after sampling. All Lifeguard-treated samples were constantly kept at 4 °C and were extracted within 3 weeks after sampling. Prior to extraction in the lab, the LifeGuard solution was removed via centrifugation according to the recommended protocol. Total RNA was extracted from approximately 2 g of soil with the RNeasy PowerSoil total RNA kit (Qiagen, Hilden, Germany). Additionally, DNA was co-extracted using the RNeasy PowerSoil DNA elution kit (Qiagen, Hilden, Germany). The final elution volume was 50 ul, and extracted RNA and DNA were stored at – 80 and – 20 °C, respectively. The total extracted DNA was used as a proxy for total microbial biomass and total RNA as a proxy for the metabolically active (i.e. protein synthesizing) microbial biomass (Blazewicz et al. 2013). Due to comparison of organic and mineral horizons and accompanied large differences in microbial biomass per gram soil

dry weight, values were normalized to SOC contents and are expressed in ng mg SOC^{-1} (Zhou et al. 1996).

Soil fractionation

Bulk soil samples went through a two-step sequential fractionation process in order to determine quality and quantity of different OM pools in permafrost-affected soils and to what extent the type of permafrost degradation affected the pools.

First, a total of 34 bulk soil samples, comprising all mineral soil horizons (excluding Dry site AhE horizon; $n = 10$) and the four Topsoil and Subsoil replicate samples from all sites ($n = 24$), were fractionated by aggregate size and divided into microaggregates (MiA) and macroaggregates (MaA) by using a modified method from Siebers et al. (2018). For that, 40 g of soil and 200 ml of ultra-pure water (1:5 w:v) were mixed on an overhead shaker for 1 h at a frequency of 20 rpm to break up all loosely attached soil particles (not water-stable aggregates). After shaking, the suspension was transferred to a 250 μm sieve, and wet sieving was done for one minute. Soil passing the 250 μm sieve was defined as MiA, while soil on top of the 250 μm sieve was considered as MaA (up to 2 mm in size). After fractionation, all samples were shock frozen in liquid nitrogen and freeze-dried. The mean \pm standard deviation (SD) mass recovery of MiA + MaA amounted to $97.9 \pm 0.9\%$ ($n = 34$). Soil OC, TN, and the $^{13}\text{C}/^{12}\text{C}$ ratio of all aggregate samples were measured by EA-IRMS. The mean (\pm SD) SOC recovery within both aggregate fractions relative to the bulk SOC amounted to $105.1 \pm 19.2\%$ ($n = 33$). The water used for fractionation was collected, quantified, and filtered through 0.45 μm polyethersulfone filters (VWR International, Darmstadt, Germany). On average (\pm SD), 423 ± 51 ml ($n = 34$) water was used per sample for the whole fractionation process. The OM released into the solution during the fractionation was considered as water-mobilizable OM, a loosely bound OM fraction and thus likely rather fast cycling. The water-extracts were stored at $+4$ °C and characterized within 2 days after fractionation by measuring the water-extractable organic carbon (WMOC) concentration by high-temperature combustion with a vario TOC cube (Elementar Analysensysteme GmbH, Hanau, Germany) and the UV absorbance at 280 nm with a SPECTROstar Nano microplate reader (BMG LABTECH Ortenberg, Germany). The UV

absorbance at 280 nm was later used to calculate the specific UV absorbance (SUVA_{280}), an indicator of the aromaticity of DOM (Kalbitz et al. 2003).

In a second step, the aggregate samples ($n_{\text{MiA}} = 34$; $n_{\text{MaA}} = 12$) were further separated into a light fraction (LF), containing POM, and a heavy fraction (HF), containing mineral-associated organic matter (MAOM), by density fractionation. Aggregate fractionation did not always yield enough MaA material for density fractionation, thus MaA sample size is smaller than MiA sample size. Typically, density fractionation is done with 20–25 g of soil (e.g. Golchin et al. 1994; Cerli et al. 2012). But since density fractionation was used after aggregate fractionation, such weights were not always feasible in this sequence. Following the descriptions of Liebmann et al. (2023a), the sample weight for density fractionation was reduced to 5 g for all aggregate samples. A few MaA samples yielded less than 5 g after aggregate fractionation, but due to comparably large LF contents, weights for density fractionation were further reduced to 1 g (Liebmann et al. 2023a). A sodium-polytungstate density solution (SPT 0, TC-Tungsten Compounds, Grub am Forst, Germany) with a density of 1.6 g cm^{-3} was used for fractionation and added to the soil in a soil:solution ratio of 1:5 (w:v), following the descriptions of Liebmann et al. (2020). In brief, soil-polytungstate mixtures were treated with ultrasound (Sonopuls HD2200, Bandelin electronic GmbH & Co KG, Berlin, Germany) to break up aggregates with an energy input of 60 J ml^{-1} (Gentsch et al. 2015). After 1 h of resting time and centrifugation at 6000 g for 30 min, the supernatant containing both free and occluded LF material was filtered through 0.45 μm PES filters (PALL Life Sciences, Ann Arbor, MI, USA). Light fraction separation was repeated once, and afterwards, the LF and the remaining HF were washed salt-free with ultra-pure water until the electric conductivities of the washing solutions were $< 10 \mu\text{S}$ for LF and $< 50 \mu\text{S}$ for HF. Washed LF and HF fractions were stored frozen (-20 °C), freeze-dried, quantified, and measured by EA-IRMS on SOC, TN, and $^{13}\text{C}/^{12}\text{C}$ ratios. The mean (\pm SD) mass recovery after MiA and MaA density fractionation amounted to $97.6 \pm 1.2\%$ ($n = 46$). Mass distributions of aggregate- and density fractions of the mineral soil horizons of the three study sites are provided in Supplementary Fig. S1. As previously reported by Liebmann et al. (2020),

the different treatments during density fractionation result in the desorption of OM to the sodium-polytungstate solution. The density solutions were filtered through 0.45 μm polyethersulfone filters, measured for OC concentrations on a varioTOC cube, and data were included in mass and OC recovery calculations. Further, washing of the heavy MAOM fractions also releases considerable amounts of OM (Gentsch et al. 2015; Liebmann et al. 2020). To account for that, the washing solutions were collected, filtered (0.45 μm polyethersulfone filter), and measured for their OC concentrations (varioTOC cube). The OC contents of the MAOM fractions were then corrected for the amounts of OC released into the solution. The mean (\pm SD) SOC recovery within MAOM and POM of the MiA fraction relative to the SOC in the MiA fraction amounted to $81.0 \pm 32.3\%$ ($n=34$). The mean (\pm SD) SOC recovery within MAOM and POM of the MaA fraction relative to the SOC in the MaA fraction amounted to $94.9 \pm 19.9\%$ ($n=12$). The total mean (\pm SD) SOC recovery as a sum of all fractions obtained by both fractionation procedures relative to the bulk SOC amounted to $94.2 \pm 14.3\%$ ($n=12$).

Calculations and statistics

The plant-available cations were calculated as the sum of Ca, Mg, K, Na, Al, Fe, and Mn measured in the Mehlich 3 extracts. The base saturation (BS, in %) was calculated according to Eq. 1:

$$BS = \frac{\sum (Ca, Mg, K, Na)}{\sum (Ca, Mg, K, Na, Al, Fe, Mn)} \times 100 \quad (1)$$

The specific UV absorbance at 280 nm ($SUVA_{280}$) was calculated as the ratio of UV absorbance and WMOC concentration ($\text{L mg C}^{-1} \text{cm}^{-1}$) (Chantigny et al. 2008).

Soil OC stocks (kg m^{-2}) were determined, either for horizons to evaluate complete profiles or for the 5 cm thick depth increments to compare Top- and Subsoils, according to Eq. 2:

$$SOC_{stock} = SOC \times BD \times depth \times 0.01, \quad (2)$$

where SOC is the soil organic carbon content in mg g^{-1} , BD is the bulk density of the fine earth fraction in g cm^{-3} , and the depth is either the horizon or increment thickness in cm. Note that there was no stone fraction (>2 mm) at the three research sites, which

would have required a correction in SOC stock calculation.

Soil profile data show individual values, while all Topsoil and Subsoil data show the mean of four field replicates \pm SD. Significant differences between Topsoil and Subsoil or between the sites were tested by analysis of variance (ANOVA, $p < 0.05$) with the Tukey test as post hoc analysis. Pearson correlation was employed to confirm the linear correlation of normal-distributed datasets (Shapiro–Wilk normality test). Statistics were done with SigmaPlot 14 (Systat Software GmbH, San Jose, USA).

Results

Mineral composition and nutrient availability

The intact permafrost soil, which serves as the reference point of a state of permafrost before degradation, featured a thick organic layer and large water contents in the active layer (both in the organic layer and the mineral soil; see Table 1). Contents of dithionite-extractable Fe provide a measure for the presence of Fe oxyhydroxides minerals with different crystallinity. Overall, Fe oxyhydroxides contents in the Intact permafrost soil were 5 \times smaller compared to the soils from both permafrost degradation sites (Fig. 2a), whereas the content of crystalline Fe phases (Fe_c), which are formed in aerated parts of the soil, highlighted the differences between the Wet and Dry site (Fig. 2b). While Fe_c decreased with depth in the soil of the Wet site, overall Fe_c contents were larger in the soil of the Dry site and additionally increased with increasing soil depth showing the largest differences between Wet and Dry site in deeper subsoils. A different trend was observable for the redox-independent Al compounds, with larger contents for the Intact soil compared to the soils of the degradation sites and a decrease in the concentration with depth for both Wet and Dry (Fig. 2c).

The mineralogical composition of soils from loess depends on the petrology of the rocks from the source area of the deposited loess, which are glacial outwash plains (in an unknown distance), and the weathering transformations during soil formation. X-ray diffraction supported by IR-spectroscopy of the <2 μm fraction of the soils under study consistently revealed that clay mineralogy is dominated by illite and

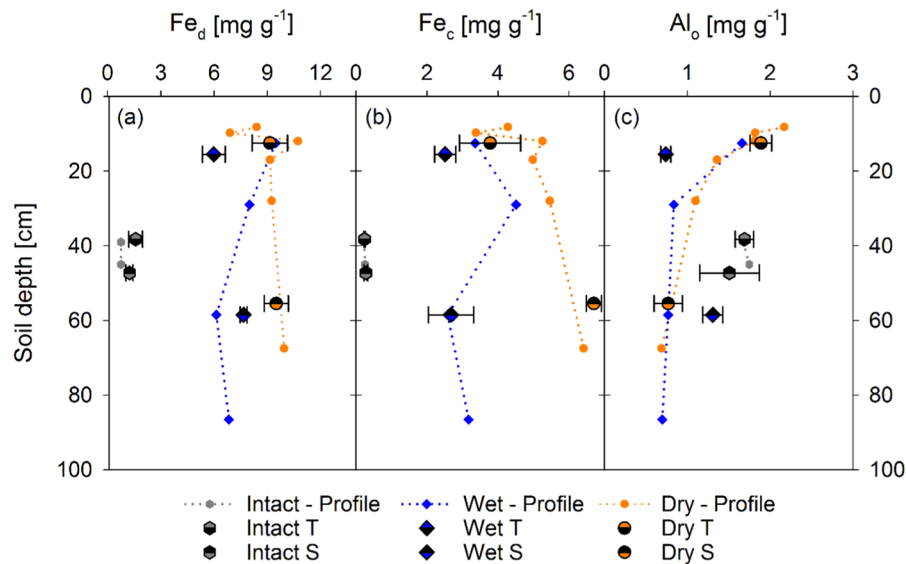


Fig. 2 Contents of dithionite-extractable iron (Fe_d), Fe in crystalline phases (Fe_c) as the difference between dithionite-extractable Fe and oxalate-extractable Fe, and oxalate-extractable aluminum (Al_o) in soils of the Intact permafrost and both degradation sites Wet (blue) and Dry (orange) are given in (a), (b), and (c) respectively. Half-colored symbols represent the

mean of Topsoil (T) and Subsoil (S) samples ($n=4$) with the standard deviation as error bars. The other data points show individual values per horizon and depth connected by dotted lines to see better the trend with depth. Please note that 0 cm soil depth refers to the soil surface and not the beginning of the mineral soil

vermiculite (Fig. 3a–c). Minor amounts of smectite, primary chlorite, kaolinite and quartz were identified. Illite, primary chlorite and quartz are typically of detritic origin. The presence of primary chlorite indicates that besides magmatic also, metamorphic rocks contributed to the loess deposited here. Illite was clearly detectable in the diffraction patterns with Mg-treatment by the discrete diffraction maximum at 1.0 nm (Fig. 3a–c). Derived from the relative intensity of interferences, illite was markedly lost in the topsoils of both permafrost degradation landscapes, where interferences at 1.40 nm most strongly indicate the extended transformation of illite to expandable layer silicates (vermiculite and smectite). For the samples with Mg and ethylene glycol treatment (Supplementary Fig. S2), interferences at 1.60 nm can be attributed to smectite, which showed discrete peaks in the two topsoil A-horizons of the Dry site and, in contrast, for the Wet site in the subsoil Br@/Cr@ horizons. In the other samples, relative intensities of smectite appeared low by forming a small shoulder on the 1.40 nm diffraction maxima towards higher d-values only. Saturation of exchange sites with K (Supplementary Fig. S3) resulted in a clear increase

of the d001 spacing at 1.0 nm, indicating contraction of vermiculite and potentially highly charged smectite upon K-uptake. The pronounced 1.40 nm peak upon heating to 550 °C can be assigned to primary chlorite, which was identifiable in all clay fractions of the horizons from Intact and Wet, whereby the interferences of primary chlorite appeared less pronounced in the samples from the Dry site (Supplementary Fig. S4). Kaolinite was clearly visible in the IR spectra by the absorption band at 3697 cm⁻¹ (Supplementary Fig. S5). Here, quartz was also identifiable by a double absorption band at 800 cm⁻¹ and in the diffraction-pattern at 0.425 nm. Both minerals, quartz and kaolinite, were present in minor amounts in all horizons determined.

Changes in mineralogical composition during the progress of soil formation can affect the release of nutrients (e.g., promoted by weathering or dissolution) as well as their retention at mineral surfaces. Plant-available cations did not differ much in the mineral soil of all profiles (Table 1). Potassium, Na, and Mn were negligible in soils of all three landscapes, whereas Al dominated at Intact and Dry Topsoil (Fig. 4a, b). Wet and Dry Subsoil showed

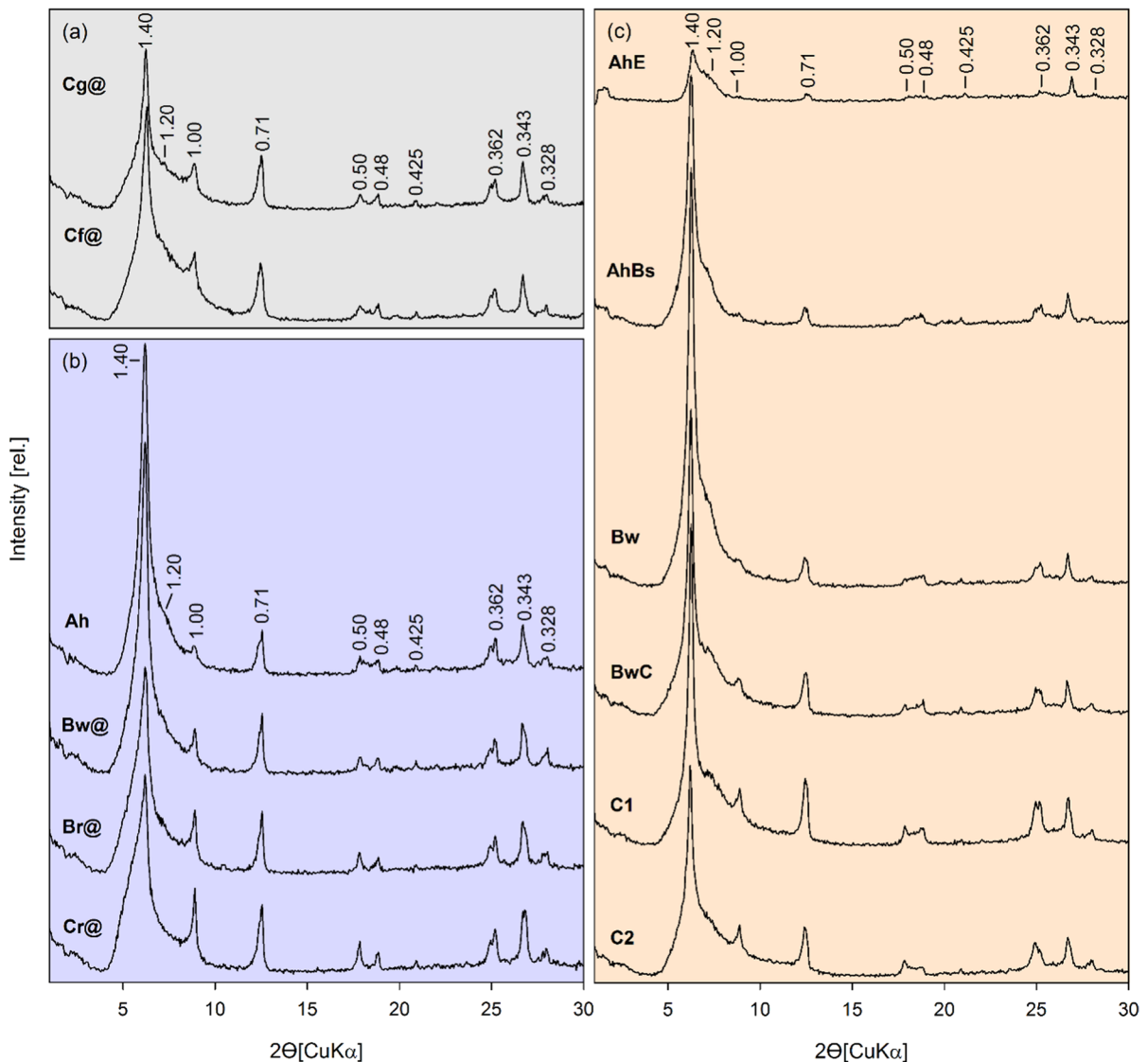


Fig. 3 X-ray diffraction patterns of the clay fraction (<2 μm) from all mineral horizons of the intact permafrost (a), Wet site (b), and Dry site (c). d-spacings in nm are given next to all distinct peaks. The Mg^{2+} -saturation treatment was chosen as discrete diffraction maxima for illite are obtained here, while The

diffraction patterns of the other treatments are given in the supplementary information, with Mg^{2+} -saturation + ethylenglycol solvation (Supplementary Fig. S2), K^{+} -saturation (Supplementary Fig. S3), and K^{+} -saturation + heating to 550 $^{\circ}\text{C}$ (Supplementary Fig. S4)

the largest availability of Mg and Ca. Base saturation exhibited no significant differences between Topsoil and Subsoil in the Intact permafrost landscape, while Topsoil in the Wet landscape had a significantly larger base saturation compared to Subsoil and vice versa for the Dry landscape (Fig. 4a, b). Thereby, differences were most pronounced for the Topsoil of both permafrost degradation sites,

with Wet Topsoil having the largest and Dry Topsoil the smallest BS (Fig. 4a).

Soil fractions

Sequential aggregate and density fractionation were employed to detect changes in SOC stabilization following permafrost degradation. Mass distribution

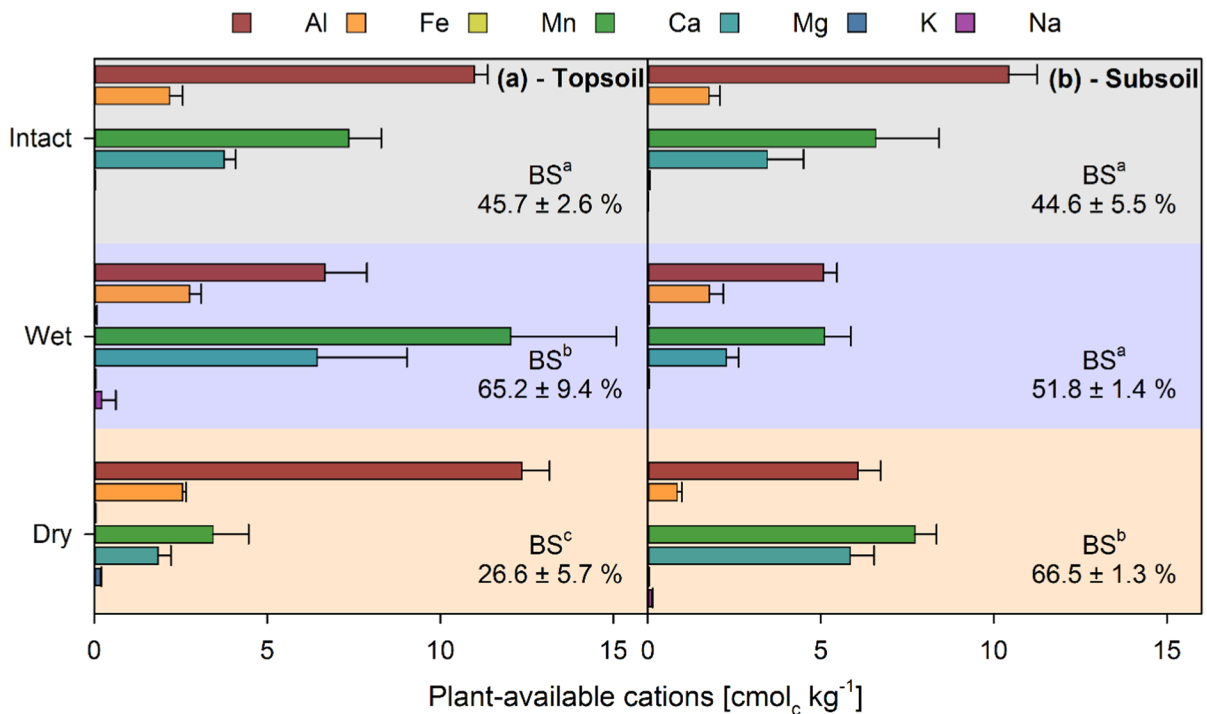


Fig. 4 Plant-available cations (aluminum (Al), iron (Fe), manganese (Mn), calcium (Ca), magnesium (Mg), potassium (K), and sodium (Na)), extracted with a Mehlich 3 solution, given for soils of the Intact permafrost (grey) and both degradation sites Wet (blue) and Dry (orange) in each case for Topsoil (a)

and Subsoil (b). Bars show the mean ($n=4$), and the error bars represent the standard deviation. The base saturation (BS) is given in each color segment as the mean \pm standard deviation, with different letters representing significant differences according to ANOVA analysis

revealed that MiA dominated throughout the sites and soil depths. At the Intact permafrost site, MiA accounted for $>95\%$ of bulk soil in Top- and Subsoil, whereas the Topsoils of the degradation sites had less MiA with $83 \pm 6\%$ at Wet and $77 \pm 10\%$ at Dry (differences not significant). The Intact permafrost soil had a small amount of MaA throughout the active layer ($<2\%$, Fig. 5 left), which is in line with the small content of crystalline Fe phases in both depths (Fig. 2b). Overall, the amount of MaA was larger in soils of both degradation sites (Fig. 5, left). The Wet site showed a large proportion of $14 \pm 9\%$ MaA in the redox-dynamic Topsoil where also more crystalline Fe phases were found (Fig. 2a, b), while in the water saturated Subsoil MaA represented only a small proportion ($1.6 \pm 0.5\%$), similar to Intact (Fig. 5, left). However, crystalline Fe contents were significantly larger in the Wet Subsoil compared to the Intact Subsoil, but still, the development of MaA was comparably small. Most MaA were found in Dry Topsoil ($21 \pm 6\%$), which

coincides with large contents of Fe phases (Fig. 2a, b). In the Subsoil, MaA contents decreased, but with $2.4 \pm 0.4\%$, they were still the largest among all landscapes showing that the Dry and Wet site led to the increase of MaA mainly in top soil horizons (Fig. 5, left).

Density fractionation of aggregate samples was done with all MiA samples and MaA from Wet and Dry Topsoil due to limited quantities of the other MaA samples. Regardless of the landscape and aggregate size, both soil depths showed that the HF dominated the mass distribution (Fig. 5, right). For MiA in the Topsoils, the smallest content of LF material was present in the Dry site ($1.1 \pm 0.4\%$), followed by the Wet site ($1.5 \pm 0.7\%$), and the Intact permafrost ($2.4 \pm 1.2\%$) (Fig. 5, right; not significantly different to each other). The Subsoils of both degradation landscapes had significantly smaller contents of LF material in the MiA compared to the intact permafrost (Fig. 5, right). Macroaggregate density fractionation revealed larger contents of LF material compared to

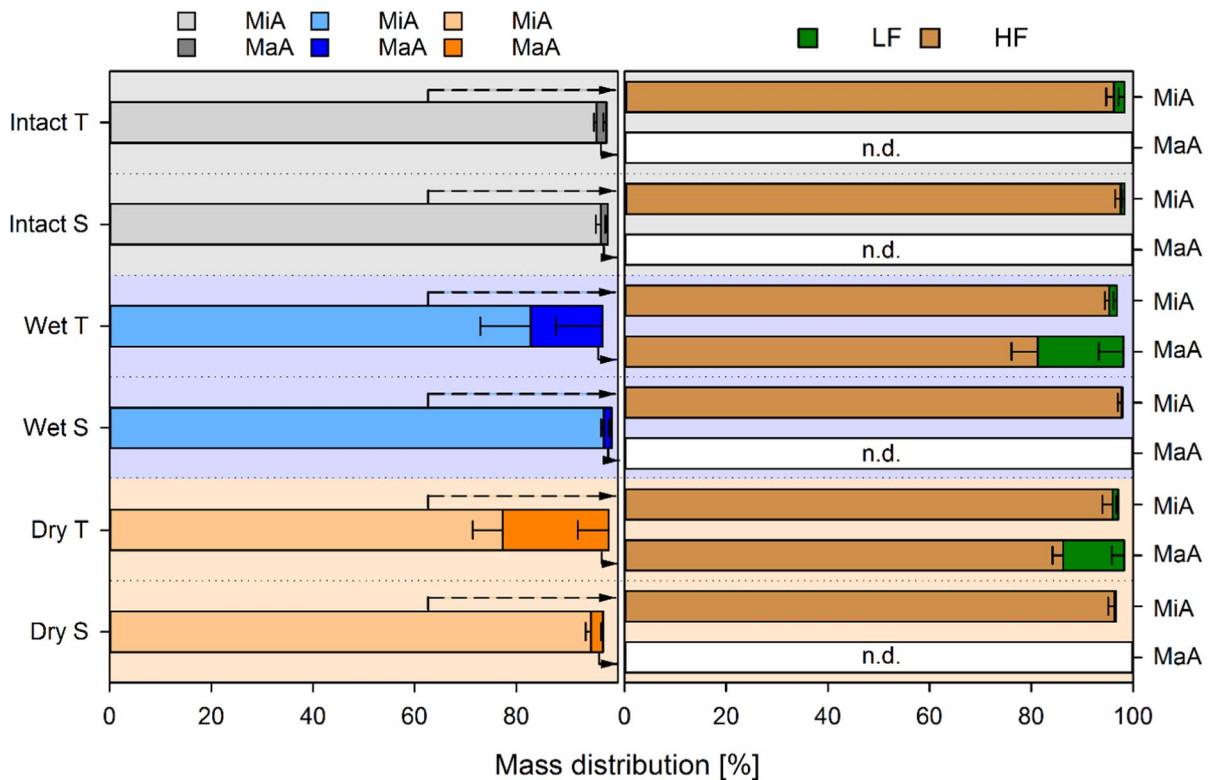


Fig. 5 Distribution of microaggregates (MiA) and macroaggregates (MaA) after aggregate fractionation for Topsoil (T) and Subsoil (S) samples of the Intact permafrost (grey) and both degradation sites Wet (blue) and Dry (orange) is given in mass-% on the left side. On the right side, the mass distribution of the light fraction (LF) and the heavy fraction (HF) after density fractionation is given within each aggregate fraction.

Black dashed arrows on the left side of the figure are marking the connection of each aggregate fraction to their respective LF/HF mass distribution. All bars represent the mean ($n=4$), with the error bars showing the standard deviation. Note that aggregate fractionation did not always yield enough (macro) aggregate material to conduct density fractionation. In such cases, n.d. (not determined) is stated for the LF/HF distribution

MiA of all soils, while most LF material was present at the Wet Topsoil MaA.

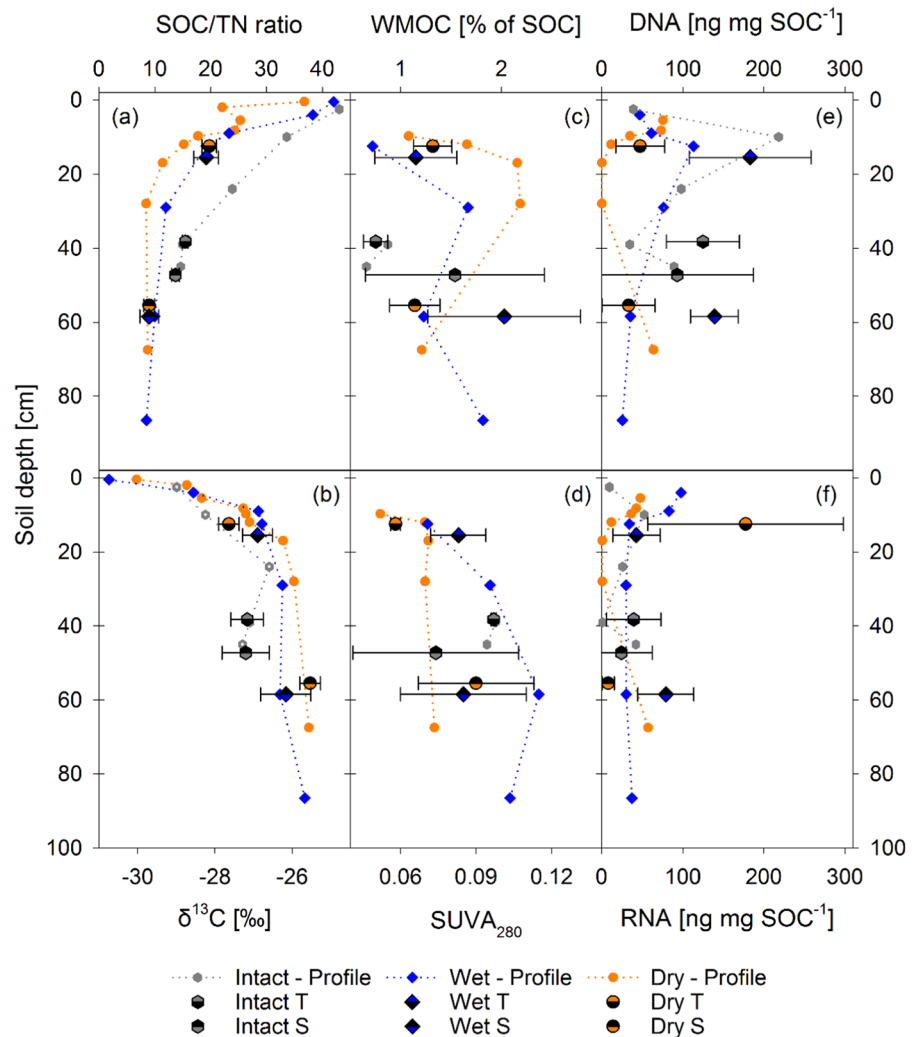
Degradation state of SOM

Carbon to nitrogen ratios, as well as $\delta^{13}\text{C}$ natural abundance of SOM in the bulk soil, varied with depth and between research sites. Generally, C/N ratios decreased from the organic layer (with ~ 40) to the mineral topsoil soil (~ 25) and further towards the mineral subsoil (~ 10 , Fig. 6a). Conversely, $\delta^{13}\text{C}$ values increased with increasing soil depth (Fig. 6b), confirmed by linear correlations (Pearson, $p < 0.05$) of both parameters (Supplementary Fig. S6). The Intact permafrost had the largest C/N ratios throughout the soil profiles and the Subsoil depths, but the C/N ratio in the intact permafrost Topsoil was smaller

compared to the Wet and Dry degraded permafrost Topsoil. Soils of both degradation landscapes depict a distinctly smaller C/N ratio in the soil profiles, in both organic layer and mineral soil, highlighting a more effective microbial decomposition, likely as a consequence of permafrost thaw (Fig. 6a). Apparently, C/N ratios in soils of the Dry and Wet sites were neither in the Topsoil, nor in the Subsoil significantly different from each other.

Water-mobilization of OC was investigated to evaluate how much SOC can be easily mobilized and leached out of the soil. Mobilization of OC was very variable, thus, differences between Top- and Subsoil and the three sites were not significant (Fig. 6c). However, a relative increase in WMOC with increasing soil depth was observable for the wet site and intact permafrost. The largest mobilization in the

Fig. 6 Depth-dependent soil organic carbon (SOC) to total nitrogen (TN) ratios in soils of the Intact permafrost (grey) and both degradation sites Wet (blue) and Dry (orange) are (a), $\delta^{13}\text{C}$ values (b), water-mobilizable organic carbon (WMOC) release relative to the SOC content (c) and specific UV absorbance at 280 nm (SUVA_{280}) (d). The latter two parameters derive from the water used for the aggregate fractionation and characterize an easily mobilizable fraction of SOC. The total microbial biomass is given in the form of DNA contents (e), whereas the active part of the microbial biomass is given as RNA contents (f). Half-colored symbols represent the mean of Topsoil (T) and Subsoil (S) samples ($n=4$) with the standard deviation as error bars. The other data points show individual values per horizon connected by dotted lines see better the trend with depth. Please note that 0 cm soil depth refers to the soil surface and not the beginning of the mineral soil



Topsoil was observed in the Dry site (Fig. 6c). Similar to WMOC proportions, also SUVA values were quite variable, and differences were not significant (Fig. 6d). Nevertheless, an overall trend of increasing SUVA values with increasing soil depth and smallest SUVA values in the soil of the Dry site were observable.

Microbial biomass using the total DNA as a proxy was calculated relative to SOC contents in the respective horizon/depth increment and is displayed in Fig. 6e. Most microbial biomass was present in the organic layers of all soil profiles, with decreasing contents in the mineral soil and with increasing soil depth. For the Top- and Subsoils, the largest

biomass was found in the Wet site in both depths, followed by the intact permafrost, whereas in the Dry site microbial biomass was smallest in both Top- and Subsoil. Considering that RNA contents can be used as proxy for the metabolically active microbial biomass (Fig. 6f), the strongest activity was found in the organic horizons. In the mineral soil, a strikingly strong activity was found in the Dry Topsoil and a strong decrease with depth, while it was vice versa in the Wet soil. For both DNA and RNA content, the Intact permafrost soil was in between the soils of Wet and Dry site, thus highlighting the effects of different hydrological conditions during permafrost degradation.

Carbon stocks

The SOC assessment for the top 100 cm of the soil profiles, encompassing organic layers but excluding litter layers, involved dividing the profile into an upper organic layer SOC stock and a mineral SOC stock. In the Intact permafrost landscape, the mineral SOC stock was further categorized into active layer mineral SOC and permafrost mineral SOC. Quantification revealed that the overall SOC content in the Intact permafrost soil exceeded that in both soils of the degradation sites by a factor of approximately 4, i.e., 43.7 kg m⁻² (Intact) compared to 10.3 kg m⁻² (Wet) and 10.8 kg m⁻² (Dry) (see Fig. 7). Considering seasonally thawed organic and mineral layers

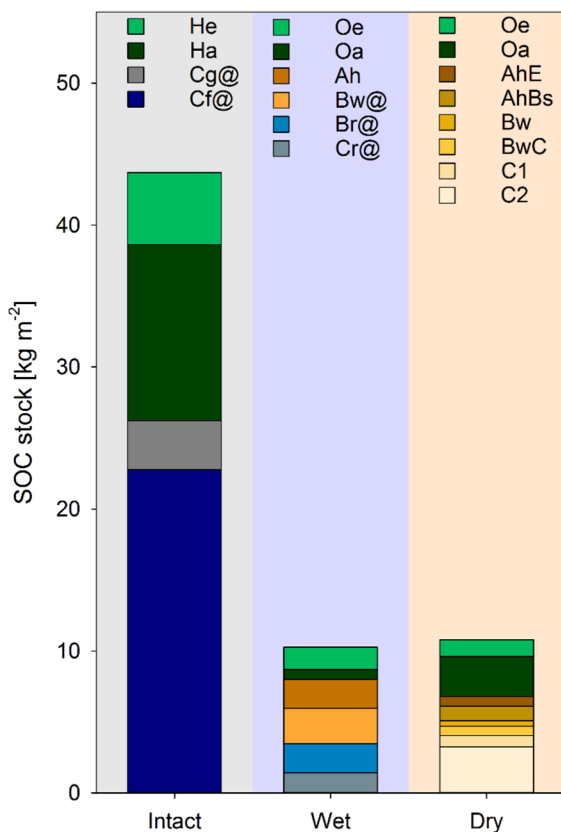


Fig. 7 Bulk soil organic carbon (SOC) stocks are given for each representative soil profile. Stocks were calculated per horizon and down to a soil depth of 100 cm. Horizon classification, as stated in Table 1, is given above each bar (IUSS Working Group WRB 2022). Note that the thickness of the active layer of the intact permafrost soil was less than 100 cm; thus the stock calculation of the Cf@ horizon was extended to 100 cm soil depth

along with the permafrost horizon highlighted that SOC storage was notably higher in all layers of the intact permafrost as compared to soils in both degraded landscapes. This includes the thick peaty organic layer, the thawed water-saturated mineral soil, and the underlying permafrost layer. Regarding both degradation sites, overall SOC stocks were comparably large, with small differences in organic layer SOC (2.3 kg m⁻² (Wet) to 4.0 kg m⁻² (Dry) and mineral horizon SOC (8.0 kg m⁻² (Wet) to 6.8 kg m⁻² (Dry) (Fig. 7). However, stock values in the mineral soil indicate that more SOC is stored under wet conditions despite smaller clay and oxyhydroxide contents compared to the Dry site soil (Table 1, Fig. 2a, b).

A more detailed look into the SOC storage of 5 cm thick Top- and Subsoil increments revealed that MiA dominated SOC storage in the intact permafrost soil throughout the active layer (Fig. 8, left). In the Topsoil of both degradation sites, SOC was evenly distributed between MiA and MaA, while the relatively small SOC stocks in the Subsoils were mainly present in the MiA fraction. The combined SOC stocks of MiA and MaA show that for both degradation sites, less SOC was stored in the Subsoil, while Topsoil SOC storage was either comparable or even greater compared to the intact permafrost (Fig. 8, left). Organic C stocks in MiA and MaA were further categorized into particulate organic carbon (POC) and mineral-associated organic carbon (MAOC) (Fig. 8, right). This breakdown emphasizes that particulate organic matter (POM) was significant contributor to SOC in both degrading and intact permafrost soils. In the Topsoils of both degradation sites, POC content exceeded MAOC, primarily within the MaA fraction. Notably, the largest POC proportions in MiA were found in the Top- and Subsoil of the intact permafrost, while little to no POC was detected in the Subsoil of the degraded soils (Fig. 8, right).

Discussion

Impact of permafrost degradation on soil development

Permafrost soils dominate arctic and subarctic regions (e.g., Hugelius et al. 2014; Ping et al. 2015). Soil development and horizon differentiation are often slow and limited to the shallow active layer due

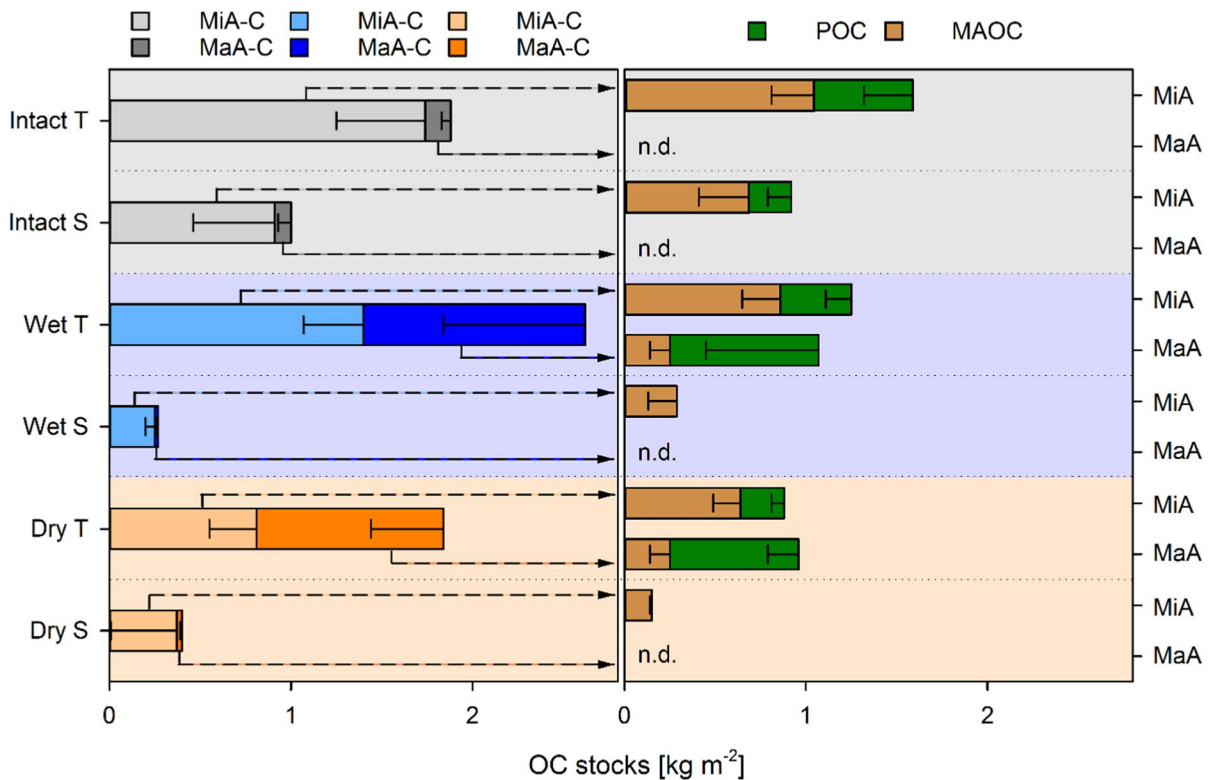


Fig. 8 Organic carbon (OC) stocks were calculated for a 5 cm depth increment in the Topsoil (T) and Subsoil (S) of the Intact permafrost (grey) and both degradation sites Wet (blue) and Dry (orange). OC stocks were differentiated into a microaggregate (MiA-C) and macroaggregate (MaA-C) share (left side) and further into particulate OC (POC) and mineral-associated OC (MAOC) within each aggregate class (right side). Black

dashed arrows on the left side of the figure are marking the connection of each aggregate fraction to their respective LF/HF mass distribution. Bars show the mean ($n=4$) with error bars representing the standard deviation. Note that not all aggregate fractions yielded enough material for subsequent density fractionation; thus POC/MAOC distribution was not always possible to determine (n.d.)

to long and cold winters combined with short summers (Munroe and Bockheim 2001; Doetterl et al. 2022). Permafrost degradation, typically linked to climate change, is better understood through the mutual influence and buffering effects of regional environmental factors such as vegetation, snow cover, and the soil organic layer (Shur and Jorgenson 2007). In the Intact permafrost landscape, the active layer thickness of 45–55 cm of the dominating Cryosols falls within the range reported by Mishra et al. (2017) and Yi et al. (2018) across Alaska or from other permafrost regions (Kokelj et al. 2002; Gentsch et al. 2015). No pronounced biochemical weathering of the parent material (i.e., transformation of clay minerals by the formation of vermiculite) in Top- compared to Subsoil within the active layer of the Intact permafrost was observed (Fig. 3a). In fact, present clay

mineralogy in the Intact permafrost is likely not of pedogenic origin, but rather inherited from the loess parent material (Borden et al. 2010). Accordingly, marginal differences between soil texture and mineralogical composition of Top- and Subsoil (Figs. 2, 3, and 4) illustrated the overall shallow active layer and pointed out the early stage of soil development and the poor differentiation of soil horizons in the active layer. Besides the formation of pedogenic minerals (oxyhydroxides and clay minerals), soil development involves the incorporation of OM and an active microbial community, which all, in turn, affect soil aggregation (Lehmann et al. 2017; Totsche et al. 2018). The Intact permafrost, however, was found to be water-saturated and thus not well aggregated, which was visible in the soil profile (Fig. 1c) and by hardly any MaA in Topsoil and Subsoil (Fig. 5, left).

This is further reflected by the limited formation of pedogenic oxyhydroxides (Fig. 2) and the not very metabolically active microbial community in the intact mineral soil (Fig. 6f). Another factor is that only small amounts of POM were present in the intact mineral soil (Fig. 5, right), particles which are considered as the nucleus for soil aggregates (Six et al. 2001; Totsche et al. 2018).

Warming of the soil promotes permafrost thaw and, thus, an active layer expansion, consequently changing the conditions for soil development accompanied by shifts in the vegetation. The conditions for soil development during permafrost degradation vary based on factors such as water release due to the melting of ground ice, inflow from the surrounding area, and the geomorphologic potential for drainage, conditions for soil development can range from wet and anoxic (“pale”) to dry and oxic (“rusty”) (Natali et al. 2015; Kwon et al. 2019; Turetsky et al. 2020). In the study area, Wet degradation resulted in a deepening of the permafrost table below the depth of 100 cm (at the Wet soil profile between 160 and 200 cm soil depth), but since cryoturbations were found within the active layer, classification of a Cryosol was still appropriate (IUSS Working Group WRB 2022). The decrease of crystalline Fe oxides from the topsoil to the subsoil (Fig. 2b) followed the soil moisture gradient (Table 1) and displayed the limited availability of oxygen under wet conditions, particularly in the subsoil. Shortage of mineral sorption sites in the Wet Subsoil can further explain the substantial decrease in plant-available cations with depth (Table 1, Fig. 4b). The transformation of illite to expandable layer silicates in the topsoil (Fig. 3) further suggest a good supply of potassium for the vegetation (Schroeder 1980). Still, since plant-available K is primarily absent (Fig. 4a, b), potassium seems to be a growth-limiting factor in the investigated soils, as it was, e.g., reported for temperate and tropical forest ecosystems (Tripler et al. 2006).

Permafrost degradation resulted in temporal aeration and growth of microbial biomass (Fig. 6e) in the Topsoil and buildup of 14% MaA, while large water contents in the Wet Subsoil largely prevented the formation of MaA (Fig. 5, left). During dry degradation, a beginning podsolization in the upper mineral soil is illustrated by $\text{pH} < 5$ (Table 1), a base saturation $< 50\%$ (Fig. 4a), and the depletion of primary chlorite (Supplementary Fig. S4), a valuable source

of magnesium, which is likewise depleted in the Dry Topsoil (Fig. 4a). Similar to the Wet site, conditions in the Dry site promoted MaA formation in the Topsoil, but not so in the Subsoil, likely due to small OM contents (Table 1) and microbial biomass (Fig. 6e). But despite having a larger MaA content in the Dry Topsoil, the incorporation of OM particles (LF material) was larger in the Wet Topsoil (Fig. 5, right), indicating a less effective decomposition of POM due to the overall larger water contents (Kwon et al. 2019). Light fraction contents, typically consisting of POM, of 2.4% (Intact), 2.0% (Wet), and 1.1% (Dry) in the Topsoil MiA fraction likewise indicated the most effective OM decomposition under oxic conditions and, in turn, the least OM stabilization for degraded and drained permafrost soils (Natali et al. 2015). Even though this trend is not significant, it indicates changes in the decomposability of OM stored in permafrost soils once degradation sets in.

Decomposition of organic matter upon permafrost thaw

Thawing of permafrost offsets the OM stabilizing conditions typical for these soils, thus triggering translocation and decomposition of SOM. Mineral horizons of the intact permafrost showed SOC contents of 22.7–27.5 mg g^{-1} , thus being in the range of SOC contents reported elsewhere (Wickland et al. 2018). However, most mineral horizons (excluding the uppermost A-horizon) accounting for $> 85\%$ of the wet and dry degraded soil profile areas had about 80% smaller SOC contents of 3.8–5.7 mg g^{-1} (Table 1). In the absence of site-specific data going back to pre-degradation times, the present study cannot attribute the differences in SOC content between intact and mined sites exclusively to dismantling effects of permafrost degradation, as inherited small-scale differences or variations in past site development may also have contributed. However, carbon contents of less degraded permafrost soils in the same environment (including the slope positions) were reported to be about 10–18 mg g^{-1} (Rooney et al. 2023), thus suggesting comparable SOC content between sites prior to permafrost degradation. This could imply that the observed differences are due to SOM mobilization during permafrost degradation, either due to microbial decomposition or leaching of DOM.

Proxies like C/N ratio and the $\delta^{13}\text{C}$ natural abundance can provide insights into the SOC decomposition stage in the intact permafrost and both degradation landscapes. Wide C/N ratios and more negative $\delta^{13}\text{C}$ values in the upper part of the soil profile illustrate inputs of fresh OM from the recent vegetation. In contrast, a strong decrease in the C/N ratio (Fig. 6a) with increasing depth underlines microbial decomposition of C-rich compounds and the release and translocation of relatively N-enriched metabolites (e.g., extracellular enzymes) to greater soil depth. Increasing $\delta^{13}\text{C}$ values with depth (Fig. 6b, Supplementary Fig. S6) are thereby connected to the isotopic discrimination of the heavier C isotope during microbial processing of SOM (Nadelhoffer and Fry 1988; Balesdent et al. 1993). Preferential sorption of C-rich but ^{13}C -depleted SOM compounds (e.g., plant-derived phenols, carboxylated lignin degradation products) in the topsoil can intensify such depth trends (Guggenberger and Zech 1994; Kaiser et al. 2001). Whereas this depth trend was found in the soils in both degradation landscapes, no differences were detected between Topsoil and Subsoil depth of the intact permafrost. Although it has to be noted that the distance between both mineral soil depths was limited to about 10 cm (whereas Dry and Wet had about 45 cm distance between Topsoil and Subsoil sampling depth), the similarities further indicate the poor soil development in the active layer. Compared to the intact permafrost soil, the larger C/N ratios in the topsoils of both Wet and Dry degraded permafrost soils do not indicate reduced decomposition. Instead, they may result from a higher incorporation of fresh POM into the Wet and Dry Topsoil (Fig. 5, right), a trend supported by the more negative $\delta^{13}\text{C}$ values. Considering the Subsoil of the three sites, the smallest C/N ratios were found in both degradation sites, suggesting that only very limited amounts of fresh or microbially processed OM reached the subsoils. This is further supported by less negative $\delta^{13}\text{C}$ values (Fig. 6b) and only minor amounts of LF material in the degraded sites subsoils (Fig. 5, right). Taken together, the data provide an indication for an advanced stage of SOM decomposition in the subsoils of the degraded sites compared to the intact permafrost, and that microbial decomposition is concentrated on the old SOM, previously protected within the permafrost.

The rather similar patterns of SOM parameters (including SOC/TN ratio, $\delta^{13}\text{C}$ values, LF material distribution) along the soil profile for the Dry site and the Wet site suggests that the decomposition of SOM after permafrost thaw is increased under both aerobic and anaerobic conditions, thus supporting findings from Xue et al. (2016). However, several incubation studies from the permafrost zone highlighted that carbon release from soil was up to 3.4 times higher under aerobic than anaerobic conditions (Schädel et al. 2016), thus suggesting that water saturation at the Wet site is more fluctuating than permanent, facilitating also temporal aerobic decomposition. Especially frequent changes in water saturation and thus redox regime in soil were found to increase microbial lignin decomposition (Liao et al. 2022). But contrary to previous reports (Kwon et al. 2019; Verbrugghe et al. 2022), a larger degree of SOM decomposition was detected in the subsoils and not in the topsoils, including the proportion of mobilizable SOM (Fig. 6c). This is further supported by the smaller C/N ratios and the less negative $\delta^{13}\text{C}$ values of Subsoil aggregate and density fractions compared to the Topsoil (Supplementary Tables S2 and S3). Enhanced vulnerability in the subsoils post permafrost thaw may be linked to a similarly large and active microbial biomass in Top- and Subsoil (Fig. 6e, f).

Overall, a comparison of an intact permafrost soil with degraded permafrost soils in different moisture conditions indicates that thawing provokes decomposition of the inherent and previously stabilized SOM.

Changes in carbon storage

Thawing permafrost can release large amounts of previously frozen OM (Turetsky et al. 2019). Previous investigations have shown that the moisture conditions after permafrost thaws and the soil depth impact SOC losses during permafrost degradation (Natali et al. 2015; Kwon et al. 2019; Estop-Aragónés et al. 2020). With about 43 kg OC m^{-2} in the upper 100 cm, the intact permafrost soil had a total SOC stock in the range of permafrost soils in other regions (Fig. 7; Ping et al. 2008; Tarnocai et al. 2009; Hugelius et al. 2014). Despite the accumulation of OM on top of the mineral soil of about 17.5 kg OC m^{-2} in form of two peat horizons (Figs. 1c, 7), the largest share of SOC was calculated for the frozen mineral soil (about 22.8 kg m^{-2} ; Fig. 7). This estimate relies

on the SOC content of 27 mg g^{-1} , measured in the upper 2–3 cm of frozen ground (approximately 50 cm soil depth, Table 1), and assumed to remain constant down to 100 cm depth. Previous studies have reported a SOC content range of 8–99 mg g^{-1} in permafrost soil cores at 74–102 cm soil depth (Wickland et al. 2018). This estimation may be conservative, as it only includes bulk soil data of the permafrost layer (Cf@), without accounting for cryoturbated topsoil material and their potentially higher SOC concentrations.

Soil OC stored in the organic layers of the degraded sites was 87% (Wet) and 77% (Dry) smaller compared to the Intact permafrost soil, suggesting pronounced decomposition of surface OM under warmer and largely oxic conditions, possibly promoted due to a shift in vegetation. An about 69% (Wet) and 74% (Dry) smaller SOC stock in the mineral horizons of both degraded sites could, to some extent, be a result of variations in initial OC contents of the loess parent material, or could largely be due to differently effective SOM stabilization mechanisms under the given site conditions. The latter further implies that there is no preferential preservation of SOC for either anoxic inhibition of microbial decomposition or oxic aggregate formation and sorptive preservation at mineral surfaces. Considering that net ecosystem respiration (sum of CO_2 and CH_4 emissions) in the Fairbanks research area can amount to a C release of about $200 \text{ g m}^{-2} \text{ yr}^{-1}$ (Ueyama et al. 2023), we infer that permafrost thaw promoted SOM decomposition within the last century can explain the majority of the detected SOC stock differences between sites. Warming and drying experiments with tundra permafrost soils in Interior Alaska likewise revealed CO_2 -C emissions up to $250 \text{ g m}^{-2} \text{ yr}^{-1}$ within one growing season (Natali et al. 2015), thus supporting our findings. Since we did not find noticeable differences between the degradation sites, our profile data contrast previous reports, where large water contents following permafrost thaw were found to stabilize SOC in the active layer better than in well-drained systems (Estop-Aragonés et al. 2020). Well-drained soils, however were reported to have accelerated SOM turnover in the upper parts of the soil profile, while decomposition in the subsoil is less affected after permafrost retreat (Göckede et al. 2019). A more detailed look at the depth distribution revealed no such SOC decrease in the Topsoil of both degradation sites (Fig. 8). Conversely, larger SOC stocks in

the 5 cm Topsoil increment of the Wet and Dry sites were observed compared to the Intact Topsoil. Aggregate- and density fractions suggest that a pronounced incorporation of POM in the Topsoil under both, wet and dry conditions (Fig. 8, right) and thus the formation of more MaA can explain larger SOC stocks in comparison to the Intact Topsoil (Figs. 5, 8, left). The shifts in vegetation from black spruce/shrubs/mosses (Intact) to black and white spruce/shrubs (Wet) to birch/aspens (Dry) is a natural succession following permafrost thaw (Van Cleve and Viereck 1981) and typically found along hillslope gradients (Jorgenson et al. 2010). Such vegetation shifts were found to be accompanied by an increase in above- and belowground biomass production (Natali et al. 2012; Douglas et al. 2014). Even though above- and belowground biomass production data were not recorded in this study, we consider this general trend as corresponding to our research area, as our soil fraction data illustrate more input of OM, especially POM, into the topsoils (Figs. 5 and 8, right). But for example due to a highly active microbial community (Fig. 6f) and thus fast SOM turnover (Schuur et al. 2008; Xue et al. 2016), SOC accumulation in the Dry Topsoil was less compared to the Wet Topsoil.

However, in comparison to the topsoil, the 5 cm thick subsoil increments showed a different picture. Largest SOC stocks were found in the Intact permafrost subsoil, as the sampling depth was at the bottom at the active layer close to the permafrost table, suggesting that the transition zone between active layer and permafrost is still a SOM accumulating and preserving environment (Shur et al. 2005; Lupachev and Gubin 2012; Ping et al. 2015). This is likely related to an accumulation of DOC from soil water percolating down to the bottom of the active layer, lower subsoil temperature, and shorter thawing period compared to the upper parts of the active layer (data not shown). Degraded permafrost landscapes showed a substantially smaller SOC storage in the Subsoil (Fig. 8). Although no data are available that show comparable SOC stocks of the three sites at the beginning of the degradation process, one reasonable explanation for the observed differences is the retreat of the preserving frozen environment to greater depth, thus increasing the output of SOC due to accelerated microbial decomposition. In addition, soil fraction-resolved C stocks demonstrate that inputs of vegetation-derived POM are not reaching deeper parts of the soil profile,

therefore suggesting that mineral subsoils can be the major net C source in thawing permafrost soils.

Conclusion

Past and recent literature provides strong evidence, based on incubations, models, and net C budgets (including this study), that permafrost thaw liberates large parts of the previously stabilized C in the soil (e.g., Schuur et al. 2008; Estop-Aragonés et al. 2020; Miner et al. 2022). Our data contribute to this relevant topic by extending the view with a soil depth- and fraction-resolved approach to unravel the complex responses of permafrost soils to environmental changes.

There is a multitude of mechanisms in the soil, which foster the stabilization of SOM against translocation and microbial decomposition after permafrost thaw. While a frozen environment prevents microbial decomposition of SOM in permafrost soils, in a well-aerated soil, SOM may be stabilized via the formation of pedogenic minerals and/or soil aggregates. In contrast, in a wet soil, anoxic inhibition of microbial decomposition may occur. However, large differences in SOC storage between intact and degraded permafrost soils suggest that these mechanisms are not equally effective, and thus, the shift in stabilization mechanisms from frozen to anoxic inhibition or oxic aggregation preserved notably less SOC than stored in an intact permafrost soil. Previous studies assigned OC losses of permafrost soils to the topsoils (e.g., Göckede et al. 2019; Kwon et al. 2019), but surprisingly our data suggest the opposite, that topsoils can even benefit from permafrost thaw due to a shift in vegetation, more biomass production, incorporation of POM in the mineral soil and formation of more macroaggregates. On the other side, subsoils were found to be the major C source during permafrost degradation since SOM is vulnerable to mobilization and microbial decomposition while there is no equivalent input of “fresh” OM. Considering whole soil profiles, subsoils account for several times the volume of topsoils. Hence, the overall C balance is, in any case, directed towards a net decline in SOC following permafrost degradation.

Acknowledgements The authors thank Roger-Michael Klatt and Till Alpmann for help in the lab. Vladimir Romanovsky

and Hana Šantrůčková are acknowledged for input during the initial project phase and Oliver Donnerhack for help with the satellite images. Financial support was provided by the Deutsche Forschungsgemeinschaft (DFG) and the Czech Science Foundation (GAČR) within the framework of the Joint German-Czech Project “CRYOVULCAN—Vulnerability of carbon in Cryosols”, with the individual grants GU 406/35-1, UR 198/4-1, VO 2111/6-1, GAČR project n. 20-21259J. We gratefully acknowledge comments from two anonymous reviewers, which helped improved the manuscript.

Author contributions The study was designed by JB, GG, TU, CV, OS, MV and PL. Field work, including identification of sites and soil sampling, was conducted by PL, JB, CV, TU, AK, and GG, while lab work was done by PL, OM, MV, MW, and HW. PL, SD, MV, and JB evaluated the data. PL wrote the first draft of the manuscript with contribution from all authors.

Funding Open Access funding enabled and organized by Projekt DEAL. This study was funded by the Deutsche Forschungsgemeinschaft (DFG) and the Czech Science Foundation (GACR) within the framework of the Joint German-Czech Project “CRYOVULCAN—Vulnerability of carbon in Cryosols”, with the individual grants GU 406/35-1, UR 198/4-1, VO 2111/6-1, GACR project n. 20-21259J.

Data availability All compiled data in this study are published in figures and tables. Detailed primary data, including bulk and soil fraction data, are published and open available in the BonaRes Repository and accessible at: <https://doi.org/10.20387/bonares-4mvd-m589> (Liebmann et al. 2023b).

Declarations

Competing interests The authors have no competing interests to declare that are relevant to the content of this article.

Open Access This article is licensed under a Creative Commons Attribution 4.0 International License, which permits use, sharing, adaptation, distribution and reproduction in any medium or format, as long as you give appropriate credit to the original author(s) and the source, provide a link to the Creative Commons licence, and indicate if changes were made. The images or other third party material in this article are included in the article’s Creative Commons licence, unless indicated otherwise in a credit line to the material. If material is not included in the article’s Creative Commons licence and your intended use is not permitted by statutory regulation or exceeds the permitted use, you will need to obtain permission directly from the copyright holder. To view a copy of this licence, visit <http://creativecommons.org/licenses/by/4.0/>.

References

- Abramoff RZ, Georgiou K, Guenet B et al (2021) How much carbon can be added to soil by sorption? *Biogeochemistry* 152:127–142. <https://doi.org/10.1007/s10533-021-00759-x>

- Atchley AL, Coon ET, Painter SL et al (2016) Influences and interactions of inundation, peat, and snow on active layer thickness. *Geophys Res Lett* 43:5116–5123. <https://doi.org/10.1002/2016GL068550>
- Balesdent J, Girardin C, Mariotti A (1993) Site-related $\delta^{13}\text{C}$ of tree leaves and soil organic matter in a temperate forest. *Ecology* 74:1713–1721. <https://doi.org/10.2307/1939930>
- Biskaborn BK, Smith SL, Noetzi J et al (2019) Permafrost is warming at a global scale. *Nat Commun* 10:264. <https://doi.org/10.1038/s41467-018-08240-4>
- Blazewicz SJ, Barnard RL, Daly RA, Firestone MK (2013) Evaluating rRNA as an indicator of microbial activity in environmental communities: limitations and uses. *ISME J* 7:2061–2068. <https://doi.org/10.1038/ismej.2013.102>
- Blume-Werry G, Milbau A, Teuber LM et al (2019) Dwelling in the deep—strongly increased root growth and rooting depth enhance plant interactions with thawing permafrost soil. *New Phytol* 223:1328–1339. <https://doi.org/10.1111/nph.15903>
- Bockheim JG, Hinkel KM (2007) The importance of “deep” organic carbon in permafrost-affected soils of arctic Alaska. *Soil Sci Soc Am J* 71:1889–1892. <https://doi.org/10.2136/sssaj2007.0070N>
- Borden PW, Ping C-L, McCarthy PJ, Naidu S (2010) Clay mineralogy in arctic tundra Gelisols, Northern Alaska. *Soil Sci Soc Am j* 74:580–592. <https://doi.org/10.2136/sssaj2009.0187>
- Carter MR, Gregorich EG (eds) (2008) Soil sampling and methods of analysis, 2nd edn. Taylor & Francis Group, Boca Raton
- Cerli C, Celi L, Kalbitz K et al (2012) Separation of light and heavy organic matter fractions in soil—testing for proper density cut-off and dispersion level. *Geoderma* 170:403–416. <https://doi.org/10.1016/j.geoderma.2011.10.009>
- Chadburn SE, Burke EJ, Cox PM et al (2017) An observation-based constraint on permafrost loss as a function of global warming. *Nat Clim Change* 7:340–344. <https://doi.org/10.1038/nclimate3262>
- Chantigny MH, Angers DA, Kaiser K, Kalbitz K (2008) Extraction and characterization of dissolved organic matter. In: Carter MR, Gregorich EG (eds) Soil sampling and methods of analysis, 2nd edn. Canadian Society of Soil Science, Taylor & Francis Group, LLC, Boca Raton, pp 617–635
- DIN ISO 11277 (2002) Soil quality—determination of particle size distribution in mineral soil material—method by sieving and sedimentation
- Doetterl S, Alexander J, Fior S et al (2022) Will accelerated soil development be a driver of arctic greening in the late 21st century?#. *J Plant Nutr Soil Sci* 185:19–23. <https://doi.org/10.1002/jpln.202100334>
- Douglas TA, Kanevskiy MZ, Romanovsky VE et al (2008) Permafrost dynamics at the Fairbanks permafrost experimental station near Fairbanks. University of Alaska, Alaska
- Douglas TA, Jones MC, Hiemstra CA, Arnold JR (2014) Sources and sinks of carbon in boreal ecosystems of interior Alaska: a review. *Elementa Science of the Anthropocene* 2:000032. <https://doi.org/10.12952/journal.elementa.000032>
- Estop-Aragonés C, Olefeldt D, Abbott BW et al (2020) Assessing the potential for mobilization of old soil carbon after permafrost thaw: a synthesis of ^{14}C measurements from the northern permafrost region. *Global Biogeochem Cycles*. <https://doi.org/10.1029/2020GB006672>
- Farquharson LM, Romanovsky VE, Cable WL et al (2019) Climate change drives widespread and rapid thermokarst development in very cold permafrost in the Canadian high arctic. *Geophys Res Lett* 46:6681–6689. <https://doi.org/10.1029/2019GL082187>
- Farquharson LM, Romanovsky VE, Kholodov A, Nicol-sky D (2022) Sub-aerial talik formation observed across the discontinuous permafrost zone of Alaska. *Nat Geosci* 15:475–481. <https://doi.org/10.1038/s41561-022-00952-z>
- Friedlingstein P, Jones MW, O’Sullivan M et al (2022) Global carbon budget 2021. *Earth Syst Sci Data* 14:1917–2005. <https://doi.org/10.5194/essd-14-1917-2022>
- Gagné KR, Ewers SC, Murphy CJ et al (2020) Composition and photo-reactivity of organic matter from permafrost soils and surface waters in interior Alaska. *Environ Sci: Processes Impacts* 22:1525–1539. <https://doi.org/10.1039/D0EM00097C>
- Gentsch N, Mikutta R, Alves RJE et al (2015) Storage and transformation of organic matter fractions in cryoturbated permafrost soils across the Siberian arctic. *Biogeochemistry* 12:4525–4542. <https://doi.org/10.5194/bg-12-4525-2015>
- Gentsch N, Wild B, Mikutta R et al (2018) Temperature response of permafrost soil carbon is attenuated by mineral protection. *Glob Change Biol* 24:3401–3415. <https://doi.org/10.1111/gcb.14316>
- Göckede M, Kwon MJ, Kittler F et al (2019) Negative feedback processes following drainage slow down permafrost degradation. *Glob Change Biol* 25:3254–3266. <https://doi.org/10.1111/gcb.14744>
- Golchin A, Oades JM, Skjemstad JO, Clarke P (1994) Study of free and occluded particulate organic matter in soils by solid state ^{13}C CP/MAS NMR spectroscopy and scanning electron microscopy. *Aust J Soil Res* 32:285–309
- Guggenberger G, Zech W (1994) Composition and dynamics of dissolved carbohydrates and lignin-degradation products in two coniferous forests, N.E. Bavaria, Germany. *Soil Biol Biochem* 26:19–27
- Heijmans MMPD, Magnússon RÍ, Lara MJ et al (2022) Tundra vegetation change and impacts on permafrost. *Nat Rev Earth Environ* 3:68–84. <https://doi.org/10.1038/s43017-021-00233-0>
- Hicks Pries CE, Schuur EAG, Vogel JG, Natali SM (2013) Moisture drives surface decomposition in thawing tundra. *J Geophys Res: Biogeosci* 118:1133–1143. <https://doi.org/10.1002/jgrg.20089>
- Hobbie SE, Schimel JP, Trumbore SE, Randerson JR (2000) Controls over carbon storage and turnover in high-latitude soils. *Glob Change Biol* 6:196–210. <https://doi.org/10.1046/j.1365-2486.2000.06021.x>
- Hugelius G, Strauss J, Zubrzycki S et al (2014) Estimated stocks of circumpolar permafrost carbon with quantified uncertainty ranges and identified data gaps. *Biogeochemistry* 11:6573–6593. <https://doi.org/10.5194/bg-11-6573-2014>

- Hut G (1987) Consultants' group meeting on stable isotope reference samples for geochemical and hydrological investigations. International Atomic Energy Agency (IAEA), Vienna
- IUSS Working Group WRB (2022) International soil classification system for naming soils and creating legends for soil maps, 4th edn. International Union of Soil Science (IUSS), Vienna
- Jin H, Huang Y, Bense VF et al (2022) Permafrost degradation and its hydrogeological impacts. *Water* 14:372. <https://doi.org/10.3390/w14030372>
- Jones BM, Grosse G, Farquharson LM et al (2022) Lake and drained lake basin systems in lowland permafrost regions. *Nat Rev Earth Environ* 3:85–98. <https://doi.org/10.1038/s43017-021-00238-9>
- Jorgenson MT, Osterkamp TE (2005) Response of boreal ecosystems to varying modes of permafrost degradation. *Can J for Res* 35:2100–2111. <https://doi.org/10.1139/x05-153>
- Jorgenson MT, Shur YL, Pullman ER (2006) Abrupt increase in permafrost degradation in Arctic Alaska. *Geophys Res Lett*. <https://doi.org/10.1029/2005GL024960>
- Jorgenson MT, Yoshikawa K, Kanevskiy M et al (2008) Permafrost characteristics of Alaska. University of Alaska, Alaska, p 5
- Jorgenson MT, Romanovsky V, Harden J et al (2010) Resilience and vulnerability of permafrost to climate change. *Can J for Res* 40:1219–1236. <https://doi.org/10.1139/X10-060>
- Jorgenson MT, Harden J, Kanevskiy M et al (2013) Reorganization of vegetation, hydrology and soil carbon after permafrost degradation across heterogeneous boreal landscapes. *Environ Res Lett* 8:035017. <https://doi.org/10.1088/1748-9326/8/3/035017>
- Kaiser K, Guggenberger G, Zech W (2001) Isotopic fractionation of dissolved organic carbon in shallow forest soils as affected by sorption. *Eur J Soil Sci* 52:585–597. <https://doi.org/10.1046/j.1365-2389.2001.00407.x>
- Kalbitz K, Schmerwitz J, Schwesig D, Matzner E (2003) Biodegradation of soil-derived dissolved organic matter as related to its properties. *Geoderma* 113:273–291. [https://doi.org/10.1016/S0016-7061\(02\)00365-8](https://doi.org/10.1016/S0016-7061(02)00365-8)
- Karjalainen O, Luoto M, Aalto J et al (2020) High potential for loss of permafrost landforms in a changing climate. *Environ Res Lett* 15:104065. <https://doi.org/10.1088/1748-9326/abafd5>
- Kleber M, Sollins P, Sutton R (2007) A conceptual model of organo-mineral interactions in soils: self-assembly of organic molecular fragments into zonal structures on mineral surfaces. *Biogeochemistry* 85:9–24. <https://doi.org/10.1007/s10533-007-9103-5>
- Kokelj SV, Smith CAS, Burn CR (2002) Physical and chemical characteristics of the active layer and permafrost, Herschel Island, western arctic coast, Canada. *Permafrost Periglac Process* 13:171–185. <https://doi.org/10.1002/ppp.417>
- Kwon MJ, Natali SM, Hicks Pries CE et al (2019) Drainage enhances modern soil carbon contribution but reduces old soil carbon contribution to ecosystem respiration in tundra ecosystems. *Glob Change Biol* 25:1315–1325. <https://doi.org/10.1111/gcb.14578>
- Lehmann A, Zheng W, Rillig MC (2017) Soil biota contributions to soil aggregation. *Nat Ecol Evol* 1:1828–1835. <https://doi.org/10.1038/s41559-017-0344-y>
- Lessovaia S, Dultz S, Goryachkin S et al (2014) Mineralogy and pore space characteristics of traprocks from Central Siberia, Russia: prerequisite of weathering trends and soil formation. *Appl Clay Sci* 102:186–195. <https://doi.org/10.1016/j.clay.2014.09.039>
- Liao C, Huang W, Wells J et al (2022) Microbe-iron interactions control lignin decomposition in soil. *Soil Biol Biochem* 173:108803. <https://doi.org/10.1016/j.soilbio.2022.108803>
- Liebmann P, Wordell-Dietrich P, Kalbitz K et al (2020) Relevance of aboveground litter for soil organic matter formation—a soil profile perspective. *Biogeosciences* 17:3099–3113. <https://doi.org/10.5194/bg-17-3099-2020>
- Liebmann P, Mewes O, Guggenberger G (2023a) Density fractionation reworked: reduce material and costs. *J Plant Nutr Soil Sci*. <https://doi.org/10.1002/jpln.202200330>
- Liebmann P, Barta J, Vogel C et al (2023b) Permafrost degradation in Interior Alaska (Data Collection). BonaRes Data Center (ZALF). <https://doi.org/10.20387/bonares-4mvd-m589>
- Liu F, Qin S, Fang K et al (2022) Divergent changes in particulate and mineral-associated organic carbon upon permafrost thaw. *Nat Commun* 13:5073. <https://doi.org/10.1038/s41467-022-32681-7>
- Lupachev AV, Gubin SV (2012) Suprapermafrost organic-accumulative horizons in the tundra cryozems of northern Yakutia. *Eurasian Soil Sc* 45:45–55. <https://doi.org/10.1134/S1064229312010115>
- Mack MC, Walker XJ, Johnstone JF et al (2021) Carbon loss from boreal forest wildfires offset by increased dominance of deciduous trees. *Science* 372:280–283. <https://doi.org/10.1126/science.abf3903>
- McKeague JA, Day JH (1966) Dithionite and oxalate-extractable Fe and Al as aids in differentiating various classes of soils. *Can J Soil Sci* 46:13–22. <https://doi.org/10.4141/cjss66-003>
- Mehlich A (1984) Mehlich 3 soil test extractant: a modification of Mehlich 2 extractant. *Commun Soil Sci Plant Anal* 15:1409–1416. <https://doi.org/10.1080/00103628409367568>
- Mehra OP, Jackson ML (1960) Iron oxide removal from soils and clays by a dithionite–citrate system buffered with sodium bicarbonate. In: Ingerson E (ed) *Clays and clay minerals*. Pergamon, New York, pp 317–327
- Miner KR, Turetsky MR, Malina E et al (2022) Permafrost carbon emissions in a changing arctic. *Nat Rev Earth Environ* 3:55–67. <https://doi.org/10.1038/s43017-021-00230-3>
- Mishra U, Drewniak B, Jastrow JD et al (2017) Spatial representation of organic carbon and active-layer thickness of high latitude soils in CMIP5 earth system models. *Geoderma* 300:55–63. <https://doi.org/10.1016/j.geoderma.2016.04.017>
- Moore DM, Reynolds RC (1997) *X-ray diffraction and the identification and analysis of clay minerals*. Oxford University Press, Oxford
- Munroe JS, Bockheim JG (2001) Soil development in low-arctic tundra of the Northern Brooks Range, Alaska, U.S.A.

- Arct Antarct Alp Res 33:78–87. <https://doi.org/10.1080/15230430.2001.12003407>
- Nadelhoffer KJ, Fry B (1988) Controls on natural nitrogen-15 and carbon-13 abundances in forest soil organic matter. *Soil Sci Soc Am J* 52:1633–1640. <https://doi.org/10.2136/sssaj1988.03615995005200060024x>
- Natali SM, Schuur EAG, Rubin RL (2012) Increased plant productivity in Alaskan tundra as a result of experimental warming of soil and permafrost: increased plant productivity in Alaskan tundra. *J Ecol* 100:488–498. <https://doi.org/10.1111/j.1365-2745.2011.01925.x>
- Natali SM, Schuur EAG, Mauritz M et al (2015) Permafrost thaw and soil moisture driving CO₂ and CH₄ release from upland tundra. *J Geophys Res Biogeosci* 120:525–537. <https://doi.org/10.1002/2014JG002872>
- Newberry RJ, Bundtzen TK, Claudice KH et al (1996) Preliminary geologic map of the Fairbanks mining district, Alaska. Alaska Division of Geological and Geophysical Surveys, Fairbanks
- Nitzbon J, Westermann S, Langer M et al (2020) Fast response of cold ice-rich permafrost in northeast Siberia to a warming climate. *Nat Commun* 11:2201. <https://doi.org/10.1038/s41467-020-15725-8>
- O'Donnell JA, Jorgenson MT, Harden JW et al (2012) The effects of permafrost thaw on soil hydrologic, thermal, and carbon dynamics in an Alaskan Peatland. *Ecosystems* 15:213–229. <https://doi.org/10.1007/s10021-011-9504-0>
- Ogden EL, Cumming SG, Smith SL et al (2023) Permafrost thaw induces short-term increase in vegetation productivity in northwestern Canada. *Glob Change Biol* 29:5352–5366. <https://doi.org/10.1111/gcb.16812>
- Olefeldt D, Goswami S, Grosse G et al (2016) Circumpolar distribution and carbon storage of the thermokarst landscapes. *Nat Commun* 7:13043. <https://doi.org/10.1038/ncomms13043>
- Opfergelt S (2020) The next generation of climate model should account for the evolution of mineral-organic interactions with permafrost thaw. *Environ Res Lett* 15:091003. <https://doi.org/10.1088/1748-9326/ab9a6d>
- Péwé TL (1954) Effect of permafrost on cultivated fields, Fairbanks Area, Alaska. Government Printing Office, Alaska
- Ping C-L, Michaelson GJ, Jorgenson MT et al (2008) High stocks of soil organic carbon in the North American Arctic region. *Nature Geosci* 1:615–619. <https://doi.org/10.1038/ngeo284>
- Ping CL, Jastrow JD, Jorgenson MT et al (2015) Permafrost soils and carbon cycling. *Soil* 1:147–171. <https://doi.org/10.5194/soil-1-147-2015>
- Post E, Alley RB, Christensen TR et al (2019) The polar regions in a 2 °C warmer world. *Sci Adv*. <https://doi.org/10.1126/sciadv.aaw9883>
- Rieger S, Dement JA, Sanders D (1963) Soil survey—Fairbanks area Alaska. U.S. Department of Agriculture, Soil Conservation Service, Alaska
- Rooney EC, Bailey VL, Patel KF et al (2023) Topography and canopy cover influence soil organic carbon composition and distribution across a forested hillslope in the discontinuous permafrost zone. *Permafrost Periglac* 34:331–358. <https://doi.org/10.1002/ppp.2200>
- Schädel C, Bader MK-F, Schuur EAG et al (2016) Potential carbon emissions dominated by carbon dioxide from thawed permafrost soils. *Nat Clim Change* 6:950–953. <https://doi.org/10.1038/nclimate3054>
- Schroeder D (1980) Structure and weathering of potassium containing minerals. Potassium in the soil/plant root system. International Potash Institute, Worblaufen-Bern, pp 5–25
- Schuur EAG, Bockheim J, Canadell JG et al (2008) Vulnerability of permafrost carbon to climate change: implications for the global carbon cycle. *Bioscience* 58:701–714. <https://doi.org/10.1641/B580807>
- Schuur EAG, McGuire AD, Schädel C et al (2015) Climate change and the permafrost carbon feedback. *Nature* 520:171–179. <https://doi.org/10.1038/nature14338>
- Sheldrick BH, McKeague JA (1975) A comparison of extractable Fe and Al data using methods followed in the USA and Canada. *Can J Soil Sci* 55:77–78. <https://doi.org/10.4141/cjss75-012>
- Shur YL, Jorgenson MT (2007) Patterns of permafrost formation and degradation in relation to climate and ecosystems. *Permafrost Periglac Process* 18:7–19. <https://doi.org/10.1002/ppp.582>
- Shur Y, Hinkel KM, Nelson FE (2005) The transient layer: Implications for geocryology and climate-change science. *Permafrost Periglac Process* 16:5–17. <https://doi.org/10.1002/ppp.518>
- Siebers N, Abdelrahman H, Krause L, Amelung W (2018) Bias in aggregate geometry and properties after disintegration and drying procedures. *Geoderma* 313:163–171. <https://doi.org/10.1016/j.geoderma.2017.10.028>
- Six J, Guggenberger G, Paustian K et al (2001) Sources and composition of soil organic matter fractions between and within soil aggregates. *Eur J Soil Sci* 52:607–618. <https://doi.org/10.1046/j.1365-2389.2001.00406.x>
- Tarnocai C, Canadell JG, Schuur EAG et al (2009) Soil organic carbon pools in the northern circumpolar permafrost region. *Global Biogeochem Cycles*. <https://doi.org/10.1029/2008GB003327>
- Textor SR, Wickland KP, Podgorski DC et al (2019) Dissolved organic carbon turnover in permafrost-influenced watersheds of Interior Alaska: molecular insights and the priming effect. *Front Earth Sci* 7:275. <https://doi.org/10.3389/feart.2019.00275>
- Totsche KU, Amelung W, Gerzabek MH et al (2018) Microaggregates in soils. *J Plant Nutr Soil Sci* 181:104–136. <https://doi.org/10.1002/jpln.201600451>
- Tripler CE, Kaushal SS, Likens GE, Todd Walter M (2006) Patterns in potassium dynamics in forest ecosystems. *Ecol Lett* 9:451–466. <https://doi.org/10.1111/j.1461-0248.2006.00891.x>
- Turetsky MR, Abbott BW, Jones MC et al (2019) Permafrost collapse is accelerating carbon release. *Nature* 569:32–34. <https://doi.org/10.1038/d41586-019-01313-4>
- Turetsky MR, Abbott BW, Jones MC et al (2020) Carbon release through abrupt permafrost thaw. *Nat Geosci* 13:138–143. <https://doi.org/10.1038/s41561-019-0526-0>
- Ueyama M, Iwata H, Endo R, Harazono Y (2023) Methane and carbon dioxide emissions from the forest floor of a black spruce forest on permafrost in interior Alaska. *Polar Sci* 35:100921. <https://doi.org/10.1016/j.polar.2022.100921>
- Van Cleve K, Viereck LA (1981) Forest succession in relation to nutrient cycling in the boreal forest of Alaska. In:

- West DC, Shugart HH, Botkin DB (eds) Forest succession: concepts and application. Springer, New York, pp 185–211
- Verbrugghe N, Leblans NIW, Sigurdsson BD et al (2022) Soil carbon loss in warmed subarctic grasslands is rapid and restricted to topsoil. *Biogeosciences* 19:3381–3393. <https://doi.org/10.5194/bg-19-3381-2022>
- Waldrop MP, Wickland KP, White Iii R et al (2010) Molecular investigations into a globally important carbon pool: permafrost-protected carbon in Alaskan soils. *Glob Change Biol.* <https://doi.org/10.1111/j.1365-2486.2009.02141.x>
- Wang Y, Wang H, He J-S, Feng X (2017) Iron-mediated soil carbon response to water-table decline in an alpine wetland. *Nat Commun* 8:15972. <https://doi.org/10.1038/ncomms15972>
- Wickland KP, Waldrop MP, Aiken GR et al (2018) Dissolved organic carbon and nitrogen release from boreal Holocene permafrost and seasonally frozen soils of Alaska. *Environ Res Lett* 13:065011. <https://doi.org/10.1088/1748-9326/aac4ad>
- Wilson FH, Hults CP, Mull CG, Karl SM (2015) Geologic map of Alaska. U.S. Department of the Interior, U.S. Geological Survey, Alaska
- Xue K, Yuan MM, Shi ZJ et al (2016) Tundra soil carbon is vulnerable to rapid microbial decomposition under climate warming. *Nat Clim Change* 6:595–600. <https://doi.org/10.1038/nclimate2940>
- Yi Y, Kimball JS, Chen RH et al (2018) Characterizing permafrost active layer dynamics and sensitivity to landscape spatial heterogeneity in Alaska. *Cryosphere* 12:145–161. <https://doi.org/10.5194/tc-12-145-2018>
- Zandt MH, Liebner S, Welte CU (2020) Roles of thermokarst lakes in a warming world. *Trends Microbiol* 28:769–779. <https://doi.org/10.1016/j.tim.2020.04.002>
- Zhou J, Bruns MA, Tiedje JM (1996) DNA recovery from soils of diverse composition. *Appl Environ Microbiol* 62:316–322. <https://doi.org/10.1128/aem.62.2.316-322.1996>
- Zimov SA, Schuur EAG, Chapin FS (2006) Permafrost and the global carbon budget. *Science* 312:1612–1613. <https://doi.org/10.1126/science.1128908>

Publisher's Note Springer Nature remains neutral with regard to jurisdictional claims in published maps and institutional affiliations.